AD-A150 550 HIGH-FREQUENCY ACOUSTIC VARIABILITY IN THE ARCTIC(U) 1/1
WASHINGTON UNIV SEATTLE APPLIED PHYSICS LAB
M SCHULKIN ET AL. MAY 84 APL-UW-8312 N00014-77-C-0309
UNCLASSIFIED F/G 20/1 NL

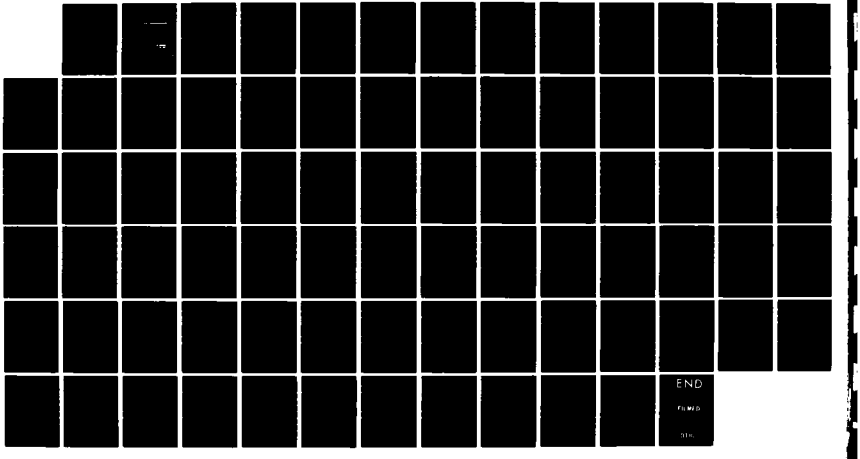

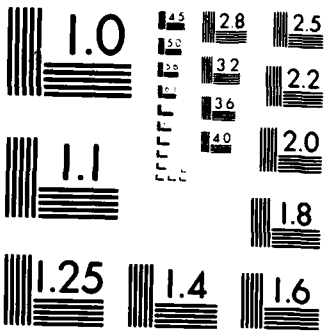

AD-A150 550

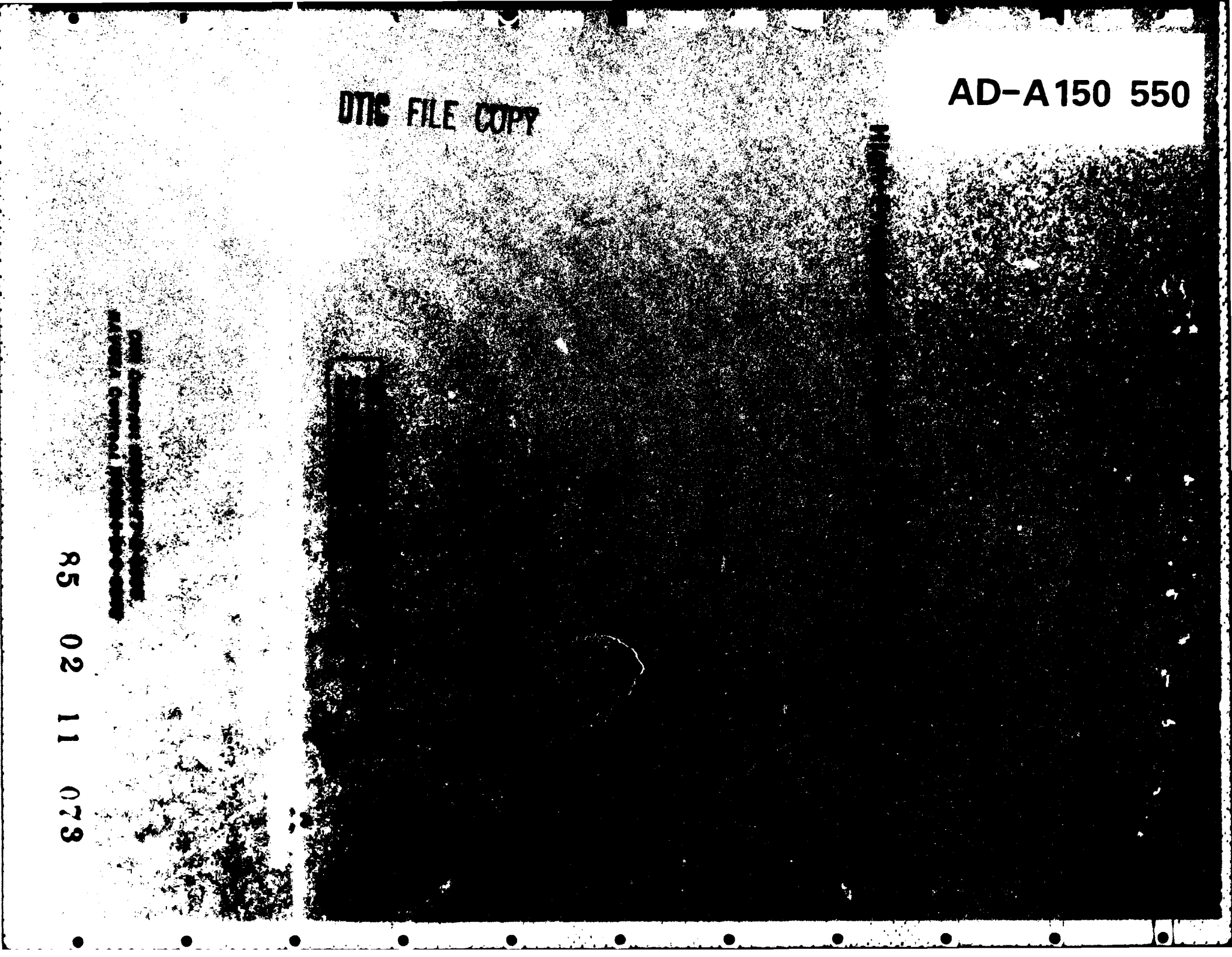

High-Frequency Acoustic Variability in the Arctic

by
M. Schulkin
G. R. Garrison
T. Wen

APL-UW 8312
May 1984

Applied Physics Laboratory University of Washington
Seattle, Washington 98105

ONR Contract N00014-77-C-0309
NAVSEA Contract N00024-81-C-6042

Acknowledgments

The authors appreciate the incisive review by Dr. S.R. Murphy, Director, and the helpful advice of Dr. T.E. Ewart of the Applied Physics Laboratory. This work was supported under ONR Contract N00014-77-C-0309 and NAVSEA Contract N00024-81-C-6042.

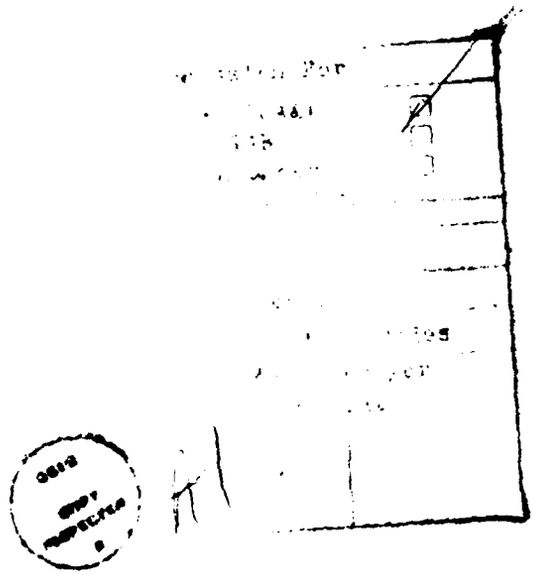

CONTENTS

ABSTRACT

Fluctuations in acoustic intensity have been studied for two locations in the Arctic – the Chukchi Sea (1974) and the Kane Basin (1979) – using the same measurement and analysis techniques. A five-frequency transducer covering the range 10-75 kHz was moved continuously in the vertical direction from 10 to 70 m. The results were used to determine the vertical correlation length and the coefficient of variation (rms variance) for the intensity at the five frequencies simultaneously. Conductivity and temperature vs depth were measured continuously before and after each set of acoustic runs. These profiles were used to construct sound ray diagrams and to compute the refractive index variance.

For direct-path propagation in both locations, it was found that when the acoustic intensity variance at low spatial wavenumbers is filtered out the remaining variance depends on the first power of the frequency and approximately the square of the range. This internal-wave-like behavior is supported by additional evidence.

The vertical correlation lengths observed for the direct-path intensity indicate that the scattering features have lifetimes longer than a few seconds and less than a few minutes. The study suggests that the scattering structures are related to anisotropic eddies that tend toward isotropy as they cascade to smaller size. Plots of a strength parameter vs a diffraction parameter show that after deterministic variations are removed from the measurements the remaining variations lie in the unsaturated direct-path region.

INTRODUCTION

For the past several years, a group at the Applied Physics Laboratory of the University of Washington has been measuring acoustic propagation beneath arctic ice floes. The original purpose of the study was to measure acoustic absorption at high frequencies (10-75 kHz) and low temperatures (−2°C) with measurements limited to direct ray paths.[1-3] Therefore, in the absorption analysis any large acoustic variations, such as those resulting from multipaths and diffraction, were eliminated. In the present study the acoustic variability is treated in detail.

High-frequency acoustic scattering and variability in the ocean and atmosphere have been studied intensively for many years. A good summary of early work is given in Refs. 4 and 5. Modern treatments are included in Refs. 6-10. Scattering and variability depend on the scale, configuration, and refractive index of the inhomogeneities as well as on the acoustic frequency. For frequencies of 10-75 kHz and propagation distances of 100-1100 m, the Fresnel radii of scattering inhomogeneities are calculated to be on the scale of oceanic finestructure, i.e., 1-10 m.

A previous study by the authors showed that a deterministic model of acoustic interaction with layered finestructure could explain a number of features of acoustic variability found in direct-path measurements in the tens-of-kilohertz range.[11] This model showed that a particular layer could dominate the acoustic variability when the transmitter and receiver were in its vicinity, i.e., at very shallow grazing angles. Layered finestructure in the ocean (which involves layers up to tens of meters in depth and up to a thousand meters or more in extent) can cause refraction effects – focusing and defocusing, ducting and antiducting – in the direct-path region. Nearly horizontal rays are affected by slowly changing multipaths which dominate the variability. At high acoustic frequencies, random variations also exist which are due to small-scale oceanic effects. These variations occur more quickly in time and space than deterministic variations and, in addition, are usually more frequency sensitive.

There are many oceanic processes occurring simultaneously at the finestructure scale which complicate a description of the acoustic environment.[12] Environmental changes occur continuously in time and space as a result of the interaction of a multiplicity of local as well as long-range energy sources with periodic as well as impulsive components. Some examples are wind, solar heating and radiative cooling, internal waves and standing oscillations, currents and current shears, and various other mixing events. All of these are thought to be related to an eddy cascade to smaller scales and final dissipation into molecular heating through viscosity.

In this report, we discuss measurements of acoustic intensity variations obtained at two locations in the Arctic – the Kane Basin and the Chukchi Sea. The measurements were taken at several frequencies simultaneously while continuously lowering or raising a set of transmitting or receiving transducers, and at several ranges. These measurements have been useful for determining the frequency and range dependence of the coefficient of variation and of the vertical correlation length.

In the analysis, an attempt is made to separate the low angle variations that are dominated by deterministic effects. This is done by removing the effects due to rays with a slope lower than a critical "ray-trapping" angle. In the case of the Chukchi Sea, this angle was about 1.5° for the projector depths used. The Kane Basin measurements showed no trapping angle. When, in addition, we filter out the low spatial wavenumber components of the intensity-depth profile to separate the remaining deterministic effects from the random effects, we find that a number of interesting results emerge. For direct-path propagation in both locations, the acoustic variance at higher spatial wavenumbers depends on the first power of the acoustic frequency and approximately the square of the range. This internal-wave-like behavior is further supported by evidence that, when the refractive index variance is calculated for the region below the halocline (40-70 m) for both the Chukchi Sea and Kane Basin data, the predicted intensity variance is compatible with internal wave theory.[6]

I. FIELD MEASUREMENTS

A. Kane Basin

The measurements in the Kane Basin were conducted from an ice floe 360 km north of Thule Air Base, Greenland, in April 1979 in water 380 m deep. CTD measurements at a lowering rate of 1.0 m s^{-1} and with a depth resolution of about 0.4 m were made before and after the acoustic runs on 10 April 1979 (see Table 1). Figure 1 shows sample profiles of temperature and salinity. Figure 2 shows the corresponding sound speed profile together with a ray diagram drawn for a source depth of 59 m. The direct-path radiation involves some caustics and interferences at a depth of 60-70 m at ranges beyond 800 m. Surface reflections arrived sufficiently later that they could be omitted by timing and are not shown.

Table 1. CTD data in support of acoustic measurements during the two field trips.

Location and Local Time of Vertical Casts		Density of Data Points (number per 60 m)	Resolution (cm/data point)[a]
Kane Basin, 1979:			
10 April	0540	146	41
10 April	1445	130	46
Chukchi Sea, 1974:			
15 April	0820	217	28
15 April	2220	220	27
18 April	1330	212	28

[a]The sampling interval was about 0.40 s. The temperature sensor response was sufficiently fast to give the stated resolution. The conductivity sensor was marginal, but adequate for determining sound speed variations.

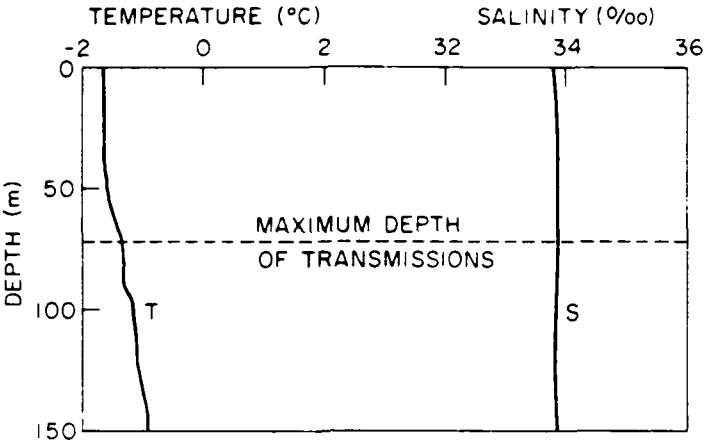

Figure 1. Temperature and salinity profiles taken at 1445 h on 10 April 1979, the day of the transmission measurements at Kane Basin.

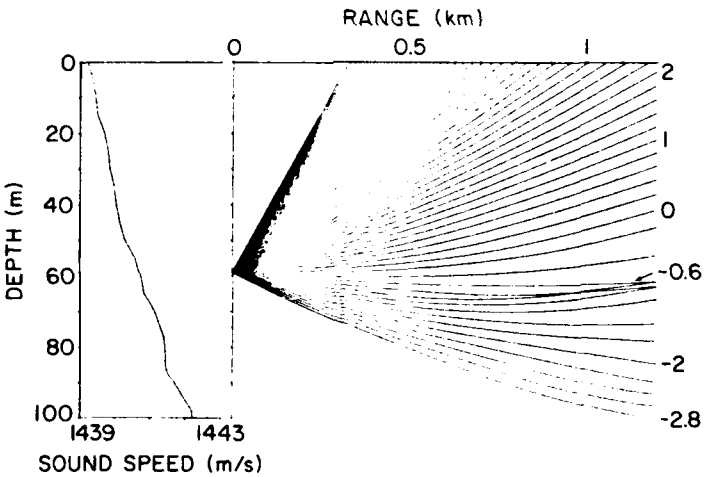

Figure 2. Sound ray diagram for a source at 59 m depth using the sound speeds calculated from the profiles of Figure 1. Rays are spaced at 0.2° from 10° to -2.8°.

Acoustic propagation measurements were made using the technique described in Ref.11 for the 1974 Chukchi Sea experiment except that in Kane Basin the receiver was fixed and the source was moved – a down-run followed by an up-run. As the 1-m long stack of source transducers was lowered or raised at a rate of about 0.5 m s^{-1}, a set of 1 ms long pulses, at frequencies of 10, 20, 30, 60, and 75 kHz and 0.1 s apart, was transmitted twice per second. The pulses were received at five fixed hydrophones (Fig. 3), providing a total of 50 intensity profiles as a continuous function of source depth between 10 and 70 m. The source's location was changed several times to give measurements at ranges of 270, 551, 820, and 1077 m. The depth resolution for the acoustic intensity runs was 0.10-0.40 m, as shown in the summary of the acoustic runs for the Kane Basin in Table 2. The data set consisting of the ten intensity profiles at each frequency was used to determine intensity spectra and intensity variance. Another advantage of using five hydrophones was that the cross-correlation could be calculated between pairs of hydrophones at different spacings.

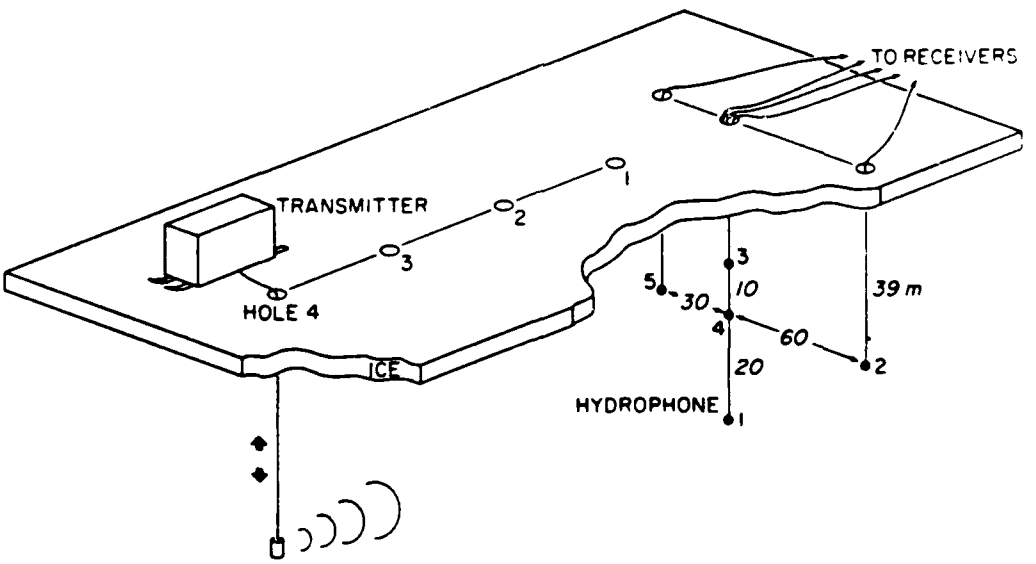

Figure 3. Arrangement of receiving hydrophones in a vertical plane perpendicular to the transmission path – Kane Basin.

Table 1. Vertical acoustic runs — Kane Basin (21 April 1973). Transmitter was moved vertically; sound was received at five hydrophones (see Fig. 3).

Range (m)	Run No.	Direction	Number of Pings for Depth Interval 10-70 m	Resolution (cm/data point)
270	21	down	329	18
	22	up	176	34
551	23	down	148	40
	24	up	223	27
820	25	down	592	10
	26	up	309	19
1077	27	down	492	12
	28	up	352	17
1077	29	down	273	22
	30	up	247	24
820	31	down	331	18
	32	up	313	19
551	33	down	391	15
	34	up	292	20
270	35	down	408	15
	36	up	164	36

Note: Set 2 (runs 29-36) was taken 9 h later than set 1.

Profiles of received intensity vs transmitter depth were plotted for all the data. In this analysis we have assumed reciprocity and have statistically treated the data collected with a moving transmitter in the Kane Basin the same as those collected with a moving receiver in the Chukchi Sea. At the shorter ranges, the pattern of the transmitting transducer reduced the intensity near the top and bottom of the profiles. To compensate for this, we have added corrections, but never more than

2 dB. A comparison of the profiles at the five frequencies (data set 1, hydrophone 1, hole 3) is shown in Fig. 4. The depth of the hydrophone is shown by a triangle. Considerable correlation between frequencies is noted. Apparently the size and strength of the inhomogeneities in the refractive index are such that the higher frequencies are affected most.

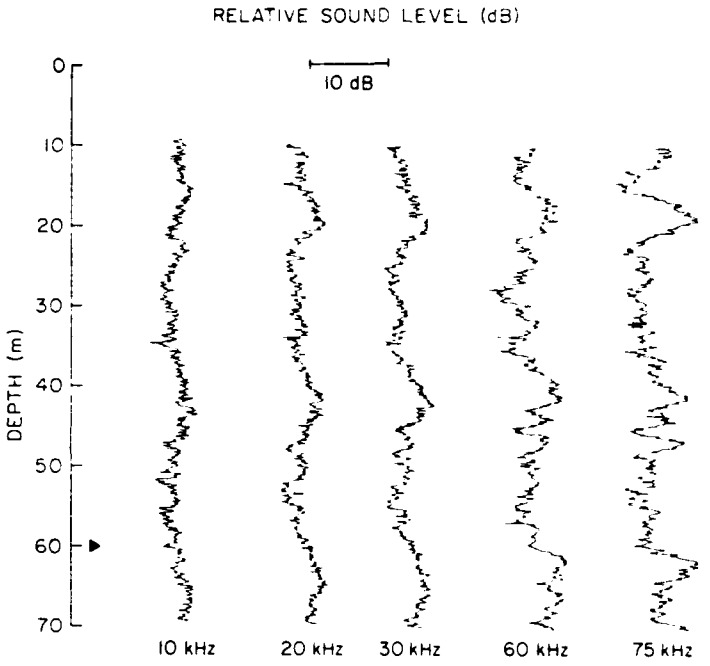

Figure 4. Example of received intensity at hydrophone 1, range 820 m, while lowering the transmitter during the first set of measurements in Kane Basin in April 1979. The receiver depth is indicated by the triangle.

A complete set of intensity profiles is included in Ref. 1. In all profiles, the vertical separation between the transmitting transducers was taken into account when calculating the depth, i.e., the depth plotted is that of the transducer element for the frequency received. Profiles are shown for the down-run and for the up-run which followed a few minutes later.

The intensity profiles at the four ranges can be compared in Figures 5a-c for signals at each of three frequencies (10, 30, and 75 kHz) received at hydrophone 1. Because there was very little correlation for small-scale (~ 1 m) variations between each down-run and the subsequent up-run, we did not expect correlation of the small-scale variations with profiles at other ranges, which were taken about an hour apart. Large-scale (5-10 m) variations were sometimes correlated but they had to last 3 h to appear at all four ranges. In this report we separate the deterministic variations of the large, extensive features and treat statistically the remaining shorter, random-like variations. Deterministic variations were of minor importance in Kane Basin, but were a major consideration in the Chukchi Sea.

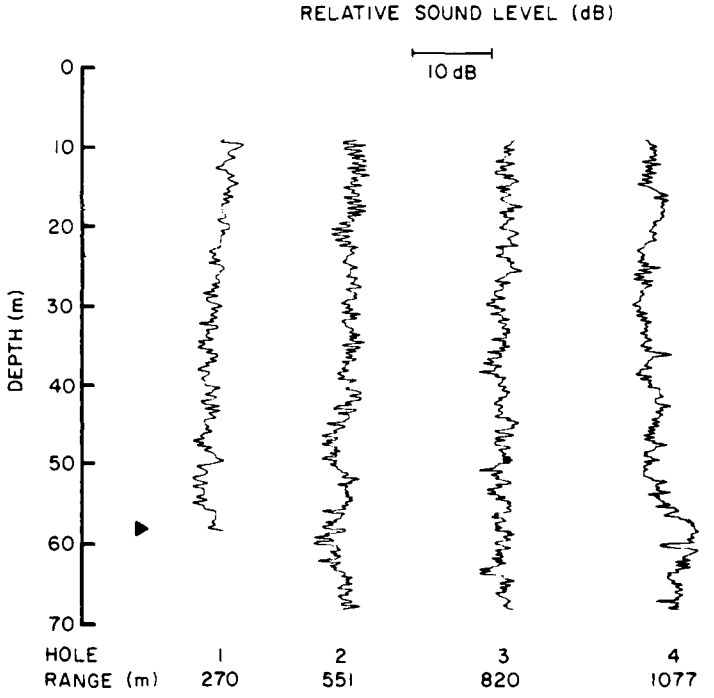

Figure 5a. Intensities at four ranges from data set 2; hydrophone 1, April 1979, frequency 10 kHz – Kane Basin.

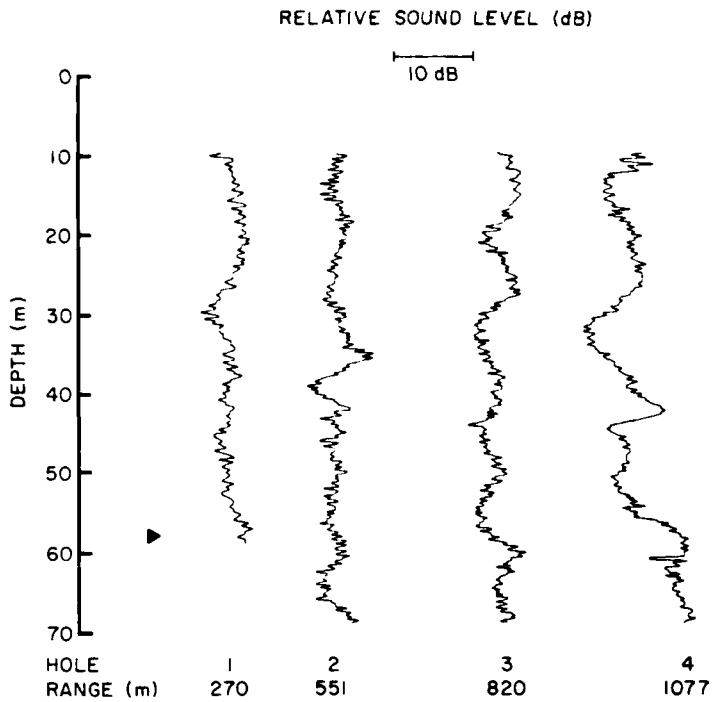

Figure 5b.

Intensities at four ranges from data set 2; hydrophone 1, April 1979, frequency 30 kHz – Kane Basin.

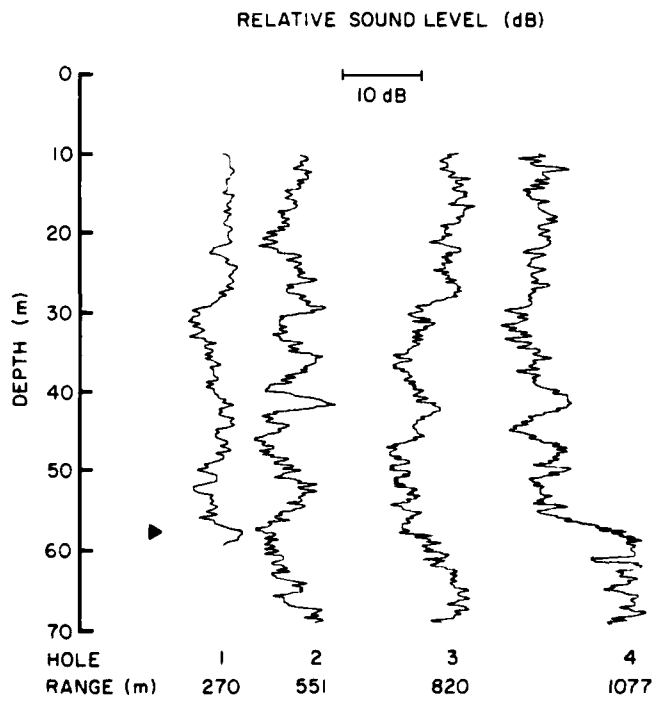

Figure 5c.

Intensities at four ranges from data set 2; hydrophone 1, April 1979, frequency 75 kHz – Kane Basin.

B. Chukchi Sea

A detailed description of the Chukchi Sea measurements in 1974 has been published previously.[11] The frequencies used were 10, 20, 30, 40, and 60 kHz, and the measurements were made at eight ranges between 190 and 1320 m. The depth resolution was about 0.08 m (two pings per second) for the intensity runs (see Table 3), whereas the resolution was about 0.28 m (two readings per second) for the supporting CTD runs (see Table 1). For these measurements, the source was at constant depth and the hydrophone was continuously lowered or raised to obtain intensity profiles vs depth. The coefficient of variation V_I (standard deviation of intensity/average intensity) for the direct-path usually reached its highest value (~1) for the 764 m measurement, and leveled off at this saturation value for greater ranges. These effects were independent of frequency and are thought to be due to the ducting and antiducting of sound caused by the intrusive layering.

Table 3. Vertical acoustic runs — Chukchi Sea (1974). Transmitter fixed; receiver was moved vertically.

Range (m)	Run No.	Number of Pings for Depth 10-70 m	Resolution (cm/data point)
		15 April	
482	18	750	8.0
	19	473	12.7
	20	667	9.0
	21	715	8.3
764	30	610	9.8
	31	701	8.5
	32	760	7.8
1041	23	715	8.3
	24	714	8.4
	25	764	7.8
1317	26	770	7.7
	27	762	7.8
	29	710	8.4
	30	610	9.8
		18 April	
193	38	715	8.3
	39	769	7.8
	40	722	8.3
364	42	735	8.1
550	47	764	7.8
	48	660	9.0
	50	725	8.2
	51	710	8.4
733	52	722	8.3
	55	689	8.7
	56	660	9.0

II. VARIABILITY OF ACOUSTIC INTENSITY

A. Introduction

In Ref. 11, we showed that, for extensive layering of the sound speed variations, the acoustic variations could be predicted from sound ray diagrams or special solutions to the wave equation. In particular, it was shown that finestructure layers 3-6 m thick and extending laterally 500-1000 m or more could cause trapping of rays with low elevation angles (~-2 to +2°). The extent of this low-angle multipath region is predictable. An example of sound speed variations and their effect on acoustic transmissions is shown in Fig. 6 for some measurements taken in the Chukchi Sea in 1972. The lower graph shows intensity anomaly in decibels; note the contrast

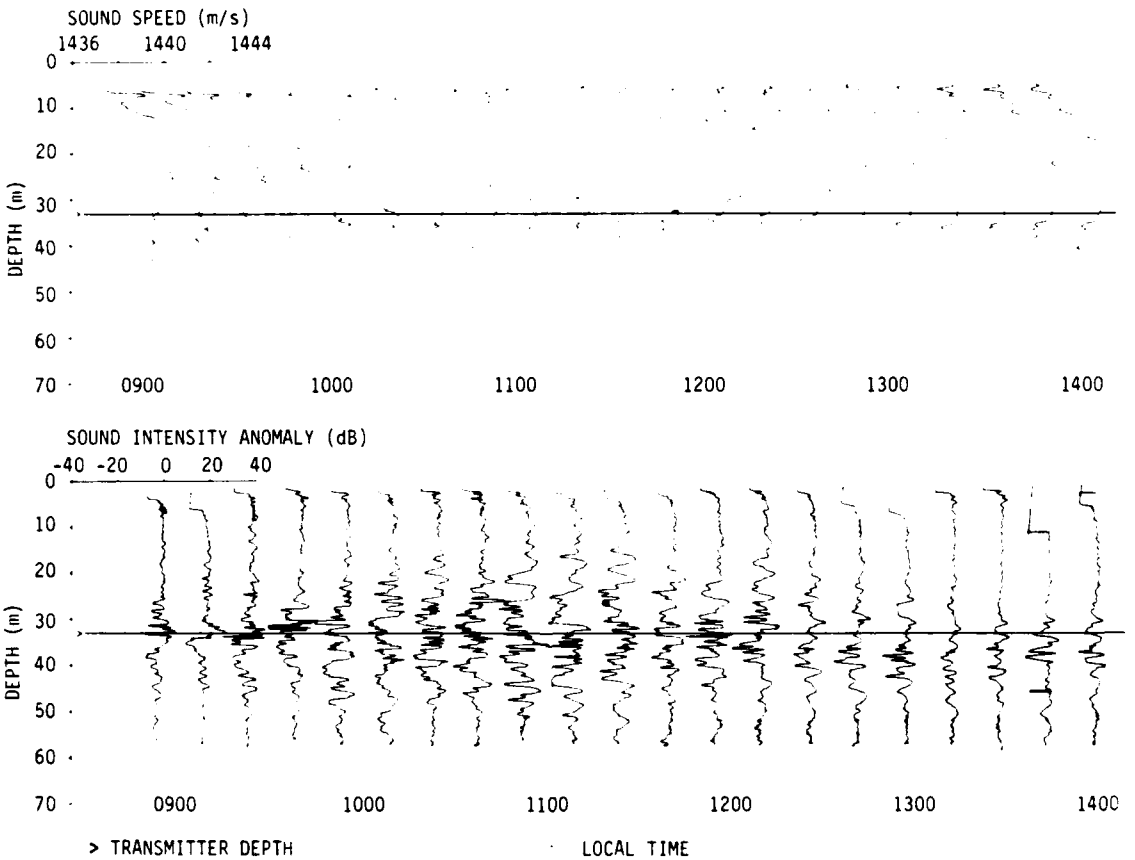

Figure 6. Simultaneous sound speed and intensity profiles taken at 15 min intervals in the Chukchi Sea in 1972. Acoustic pulses at 60 kHz were received at 300 m from the transmitter.

between the amplitude variations near the transmitter's depth and the smaller, more random variations at the higher angles. The upper graph shows the corresponding sound speed profiles; note that larger variations in the profile are fairly consistent over adjacent 15-minute sampling intervals but gradually change over longer intervals. The larger variations extend throughout the path, and their effect on propagation can be computed deterministically. The smaller variations are more random, and vary so rapidly with both time and space that they must be treated statistically.

The isolated waters in the Kane Basin are sufficiently mixed and isotropic that the statistical treatment is applicable for most of the intensity variations. The more intrusive waters of the Chukchi Sea, on the other hand, have a layered sound speed structure; the effect of these layers on propagation must be separated before the remaining smaller, random-like variations can be treated statistically.

The separation between deterministic effects, which have been treated earlier,[11] and the statistical effects, which we wish to treat here, is difficult. Our approach is to assume that the acoustic variations observed by vertical probing will be more closely spaced (i.e., have a higher spatial wavenumber) for the statistical effects than for the deterministic effects. Two methods have been applied to the problem of separating the two effects, and both are discussed here. One involves use of harmonic analysis to separate the acoustical effects into low and high spatial wavenumbers. The other requires a numerical filter to remove the effects at low spatial wavenumbers. Even though the Kane Basin data had only a small deterministic component, the data from both locations were treated by the same two methods, for consistency. An agreement between the two methods would provide confidence in the results because they are widely different in approach.

B. Methods of Data Analysis

As mentioned previously, two methods were developed for filtering out the acoustical variations at low spatial wavenumbers: (1) a harmonic analysis method, in which the acoustical effects at lower wavenumbers were separated and removed; (2) a "5-m interval method," in which only the fluctuations within each of the twelve 5-m depth intervals between 10 and 70 m were treated, thus eliminating the low-spatial-frequency variations that involved several intervals. This latter method has the additional advantage that the dependence of variability on elevation angle can be studied. The use of these two methods for identifying and removing the deterministic effects at low grazing angles is described in the following paragraphs.

1. Harmonic analysis method

An examination of the depth variability in the acoustic intensity runs listed in Table 3 showed a sizable low-spatial-wavenumber component common to all acoustic frequencies. This component was considered to be due to either refraction or frequency-independent scattering by large, stable layers or patches. It was decided to separate this component from the random, high-spatial-wavenumber component by harmonic analysis.

This method is demonstrated in Table 4. The first step is to decompose the intensity-depth profile for each acoustic frequency into spatial harmonics. By adding the spectral power in all the harmonics up to and including the N^{th} harmonic, we obtain the variance for a composite of the first N harmonics, which is shown in the left half of Table 4; similarly, each entry in the right half of Table 4 represents the variability for all harmonics above the N^{th} harmonic. The values shown are $ln(1+V_I)$, instead of the coefficient of variation V_I used elsewhere in this report, because this is the variable used in the Rytov method.

Table 4. Determination of the harmonic cutoff for frequency-independent intensity variations with depth (example: Chukchi Sea, Run 45, range 551 m).

Harmonic, N	Spatial Wavelength (m)	Variability[a] for Harmonics ≤ N, Acoustic Frequency (kHz) 10	20	30	40	60	σ_L[b]	Variability[a] for Harmonics > N, Acoustic Frequency (kHz) 10	20	30	40	60	σ_H[b]	σ_H/σ_L
0	-	-	-	-	-	-	-	0.371	0.431	0.517	0.553	0.670	0.102	-
1	60	0.059	0.200	0.051	0.081	0.020	0.062	0.368	0.400	0.516	0.530	0.670	0.107	1.73
2	30	0.227	0.329	0.281	0.257	0.324	0.039	0.315	0.317	0.467	0.495	0.628	0.118	3.02
3[c]	20	0.282	0.341	0.284	0.258	0.334	0.032	0.270	0.303	0.465	0.494	0.625	0.130	4.05
4	15	0.292	0.366	0.342	0.314	0.426	0.046	0.259	0.270	0.432	0.470	0.584	0.124	2.66
5	12	0.293	0.366	0.344	0.335	0.470	0.059	0.257	0.269	0.430	0.458	0.555	0.115	1.95
6	10	0.306	0.384	0.353	0.353	0.471	0.055	0.241	0.237	0.424	0.446	0.554	0.124	2.25
7	8.6	0.306	0.392	0.360	0.414	0.496	0.063	0.241	0.220	0.419	0.394	0.534	0.117	1.86
8	7.5	0.318	0.394	0.403	0.445	0.508	0.063	0.222	0.216	0.379	0.355	0.523	0.114	1.81
9	6.7	0.326	0.400	0.410	0.446	0.529	0.066	0.208	0.200	0.371	0.353	0.502	0.113	1.71
10	6	0.329	0.407	0.416	0.455	0.564	0.077	0.203	0.180	0.364	0.340	0.458	0.104	1.35

[a] Tabulated values are $\ln(1+V_I)$, where V_I^2 is the intensity variance and V_I is the coefficient of variation.

[b] σ_L and σ_H are the standard deviation of the five values to their left.

[c] Selected cutoff harmonic. Underlined values were used as the high-frequency variances for this run.

The dependence of the variability on acoustic frequency was examined by computing the standard deviation σ of the tabulated values for the five frequencies. This was done for both the low-spatial-wavenumber region (harmonics $\leq N$) and the high-spatial-wavenumber region (harmonics >N) to obtain the values of σ_L and σ_H listed in Table 4. A low value of σ_L indicates a weak dependence on acoustic frequency. A high value of σ_H indicates a strong dependence on acoustic frequency under the assumption that the variance in the high-frequency region increases with acoustic frequency, which did occur. The criterion for selecting the harmonic cutoff for the frequency-independent region was to choose that harmonic for which the ratio of σ_H to σ_L was a maximum (i.e., 4.05 in Table 4). The corresponding V_I for harmonics above the cutoff are underlined.

2. Five-meter interval method

In this method, V_I is determined for each 5-m interval of a vertical run. This procedure is capable of showing how variability depends on the elevation angle of the path from the source to the receiver. It is helpful in eliminating intervals containing trapped rays and acts as a filter to eliminate low-angle deterministic variations. The choice of 5 m for the interval size is somewhat arbitrary, but the interval had to be (1) large compared with the correlation length for the high-spatial-wavenumber variations, (2) large enough to contain enough individual values of V_I so that we could estimate meaningful statistical variations, and (3) small enough to provide several values of vertical angle. A problem could arise with this method if there were sudden swings in intensity within one of the 5-m intervals. The unimportance of this latter effect was verified by shifting the 5-m intervals by a meter or so and noting that the results were consistent. The variability closer to the surface seems to be complicated by complex energy interchanges.

C. Computations and Results

1. Kane Basin

The median values of V_I obtained for the Kane Basin data when using both methods are plotted in Fig. 7 on a log-log scale against frequency for each range. The use of five receiving hydrophones during each run gave a possibility of five records per run, increasing the data set by a factor of 5 for each vertical profile. The harmonic method yields somewhat larger values which may be explained as follows. Sometimes the deterministic effects include ray crossings that involve interference. This produces a frequency-dependent effect which the harmonic

method includes with the small-scale random variations, causing an increase in the values of V_I. Lines representing an $f^{1/2}$ law have been drawn, and the graphs show reasonably good agreement. Because the data at all five frequencies were taken almost simultaneously at a given range, this relationship is well determined by the experiment.

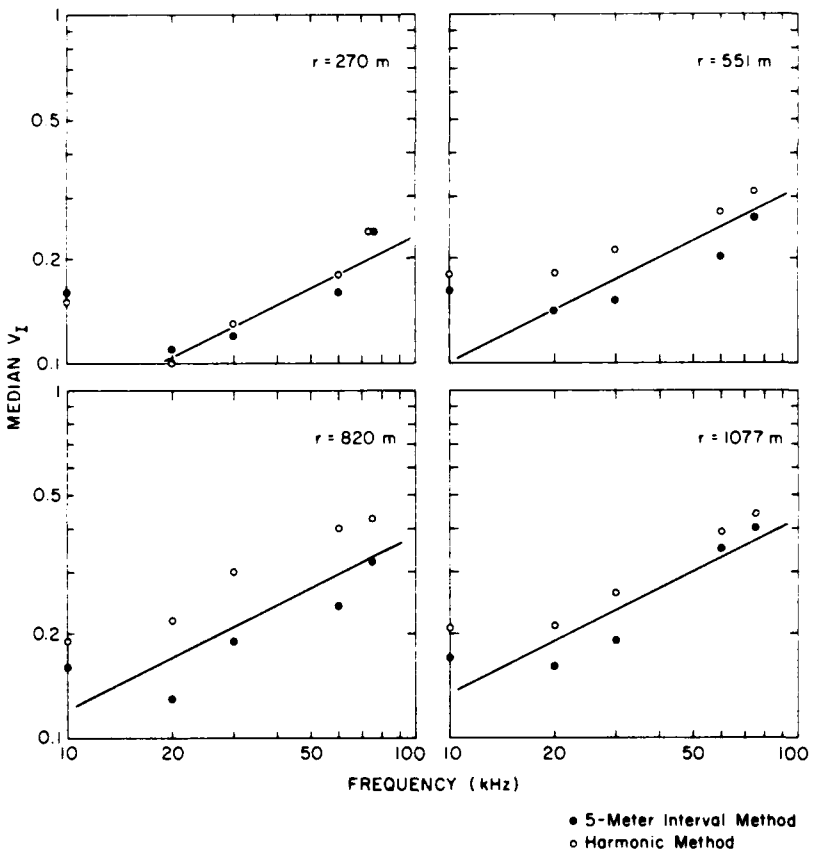

Figure 7. Coefficient of variation vs frequency as determined by two methods – Kane Basin. Lines are for a dependence of $f^{1/2}$. The V_I values plotted here are tabulated in Table A1 (the prefix "A" refers to the appendix).

In Fig. 8 the V_I data are plotted on a log-log scale against range for each frequency. Except at 10 kHz and at short range, the range dependence follows approximately a first power law to about 1000 m. This first power law behavior would be expected for these ranges if the scattering were due to random anisotropic inhomogeneities for which the statistical distribution in space and time was stationary.[13]

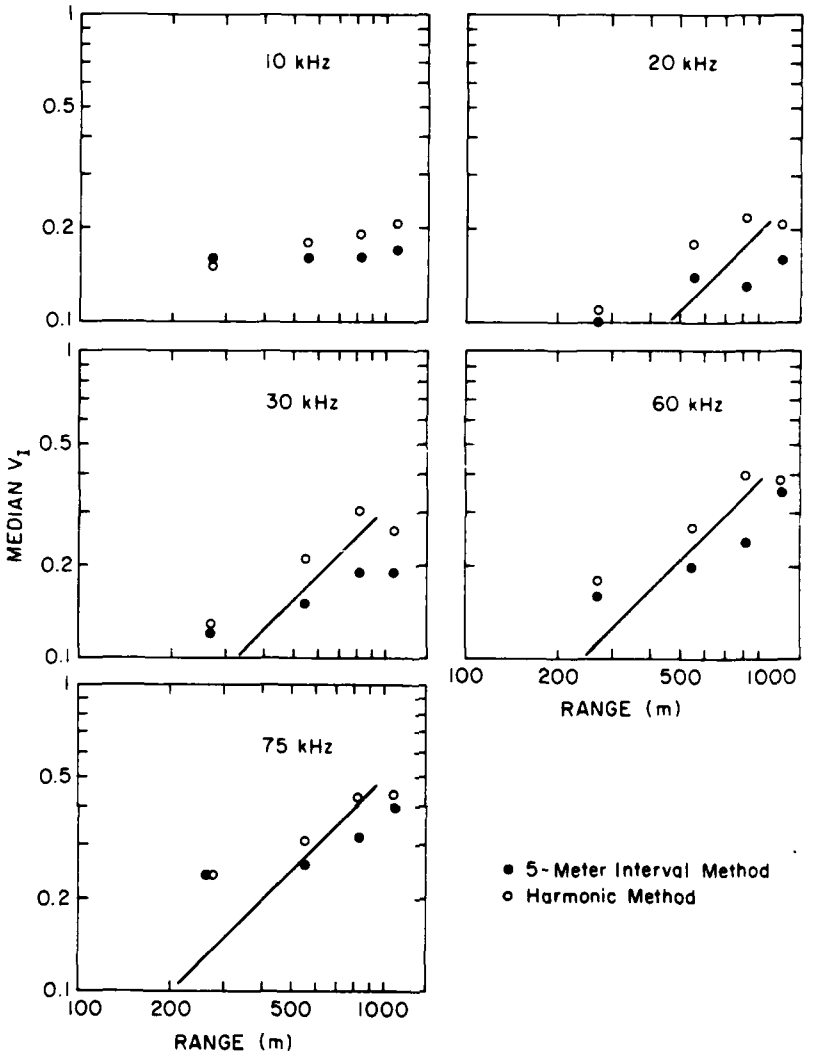

Figure 8. Coefficient of variation vs range as determined by two methods – Kane Basin (from Table A1). Lines are for linear r dependence.

2. Chukchi Sea

Figure 9 shows the median V_1 values for each range obtained by both methods for the two days of measurement, 15 and 18 April 1974. As for the Kane Basin data, the 5-m interval method yields generally lower values. The plot of V_1 vs frequency for each range (Fig. 9) again shows agreement with an $f^{1/2}$ dependence for ranges of 400 to 1000 m. At less than 400 m, there is a spreading and convergence of rays, but not enough overlapping to produce the interference that is frequency dependent. Beyond 1000 m, V_1 is so near saturation (~1.0) that little dependence on frequency is visible.

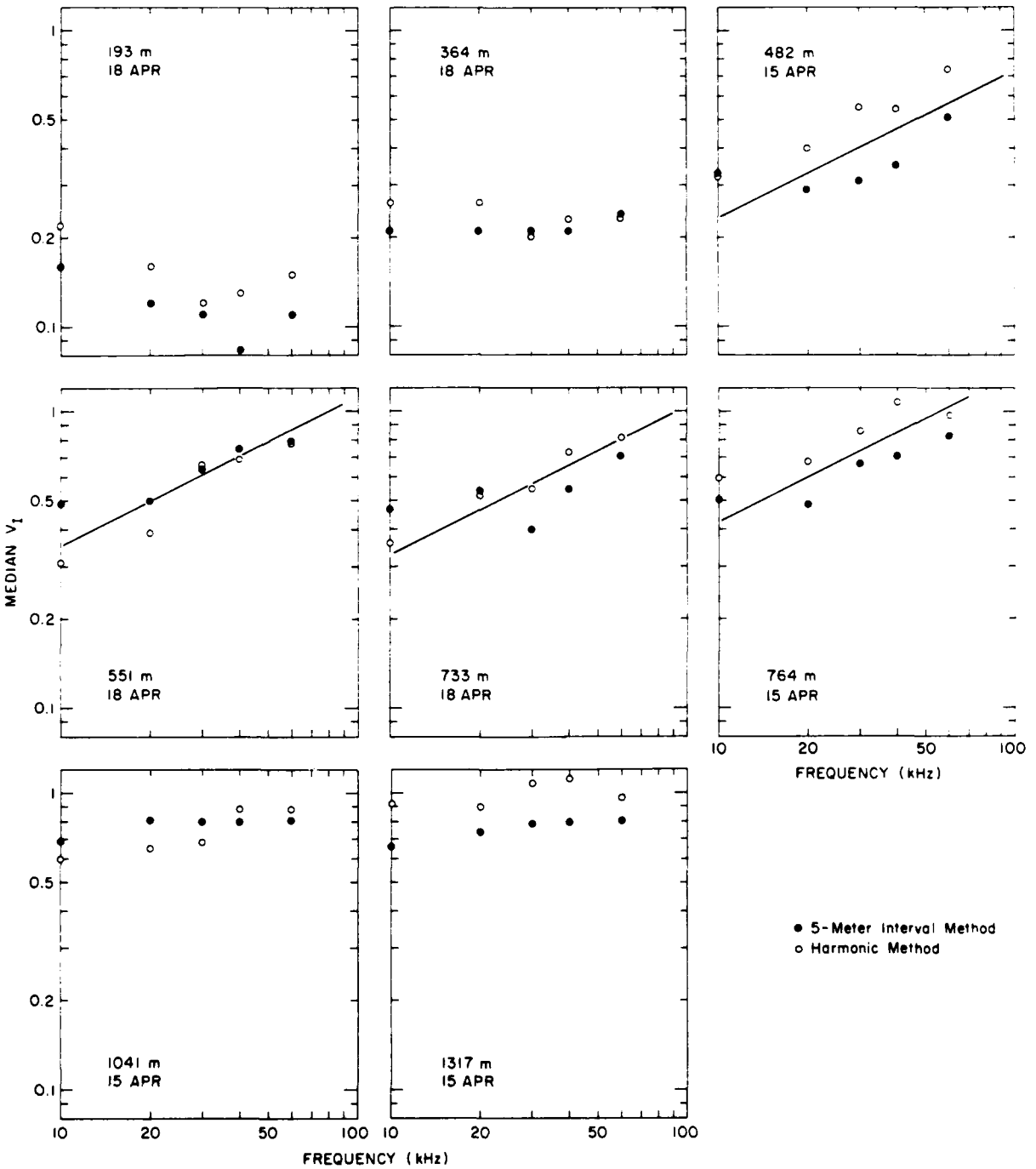

Figure 9. Coefficient of variation vs frequency as determined by two methods – Chukchi Sea. Lines are for an $f^{1/2}$ dependence. Tables A2 and A3 list the V_1 determined by each method, with a summary in Table A4.

D. Dependence of Acoustic Variability on Elevation Angle

Although the plots of the Kane Basin data did not show any dependence on elevation angle, the Chukchi Sea data showed a marked dependence. The median data for all ranges have been separated into two sets, depending on the geometric elevation angle θ: $|\theta| < 1.5°$ and $|\theta| \geq 1.5°$ and plotted in Fig. 10. In general, the set for smaller elevation angles shows considerably more acoustic variability. This difference is judged to arise from the effects of the intrusive finestructure layering in the Chukchi Sea, as discussed in Ref. 11. An $f^{1/2}$ dependence is seen for the larger angles but not for the low angles. In Fig. 11, the frequency dependence is shown for all the higher-angled rays for all the runs. An $f^{1/2}$ dependence is not apparent for the short- and long-range measurements. In Fig. 12, the range dependence of these data is presented for each frequency and is shown to follow approximately a first power law.

As stated earlier, the 5-m interval method of filtering has an important advantage over the harmonic method in that the dependence of acoustic variability on the elevation angle can be studied by comparing the twelve 5-m intervals in the 10-70 m depth interval at each range. The median V_I value for the Chukchi Sea runs has been obtained for each 5-m interval, each frequency, and *each range*. Ray bending is ignored in assigning a vertical angle to each 5-m interval. Figure 13 shows an example of the elevation angle dependence for 30 kHz at the range nearest 800 m for both locations. The separation of the data into positive (upgoing) and negative angles shows that both follow the same behavior. For the Kane Basin data, V_I is relatively small and shows no dependence on elevation angle. For the Chukchi Sea data, V_I is nearly constant for shallow angles up to about 1.5° after which it falls off as $|\theta|^{-1}$ (variance going as $|\theta|^{-2}$). Because V_I was shown in Figs. 7 and 9 to vary as $f^{1/2}$ in the falloff region, the combined behavior in this region goes as $V_I \sim f^{1/2}|\theta|^{-1}$. Cutoff elevation angles were determined similarly for other frequencies and ranges (except for the two shortest ranges, where V_I did not vary with angle or frequency) and are listed in Table 5.

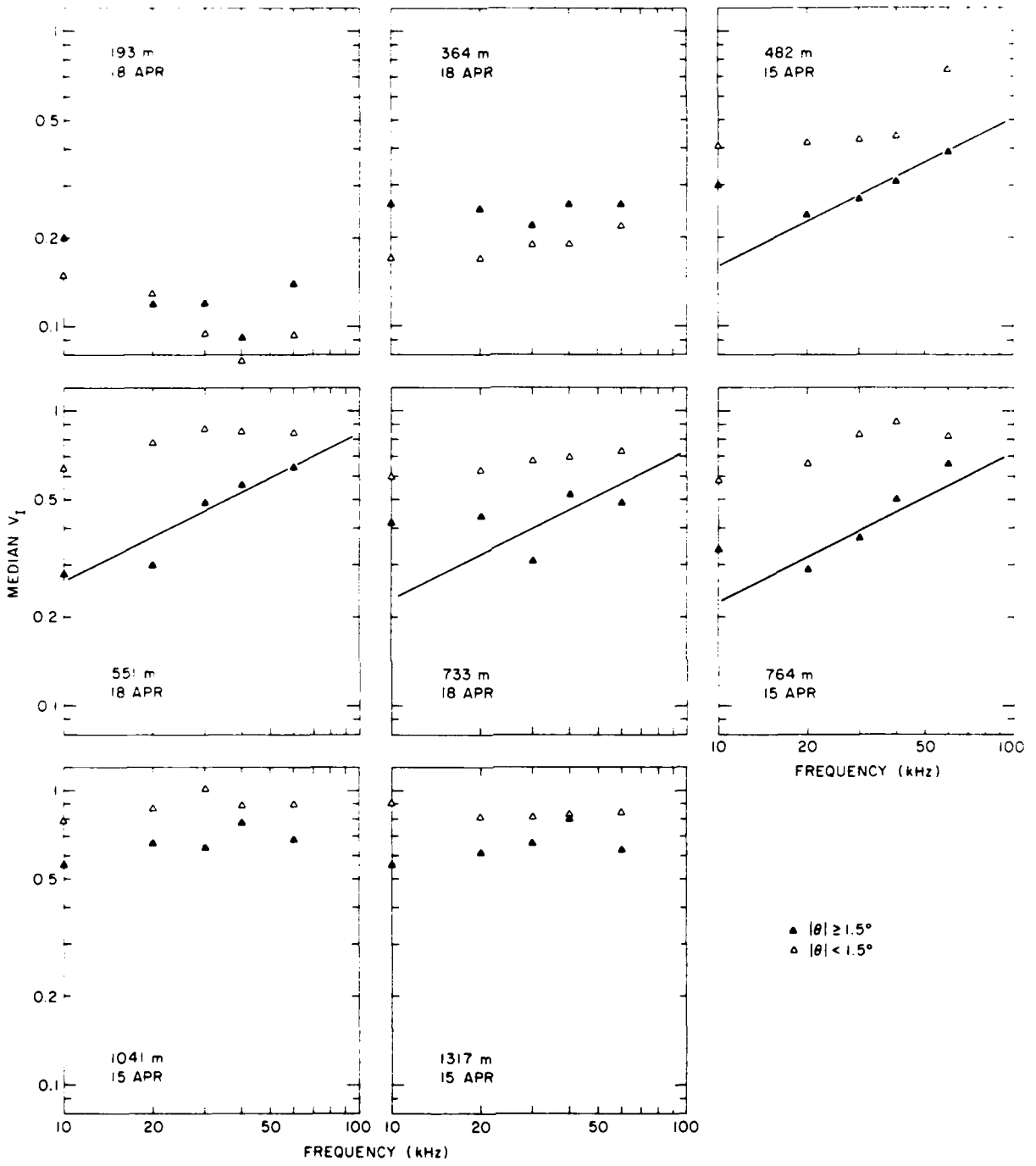

Figure 10. Coefficient of variation vs frequency as determined by 5-m interval method for two sets of elevation angles – Chukchi Sea. The V_I values are nearly independent of f for $|\theta| < 1.5°$. The lines represent an $f^{1/2}$ dependence. A tabulation of the data appears in Table A5, with medians shown in Table A6.

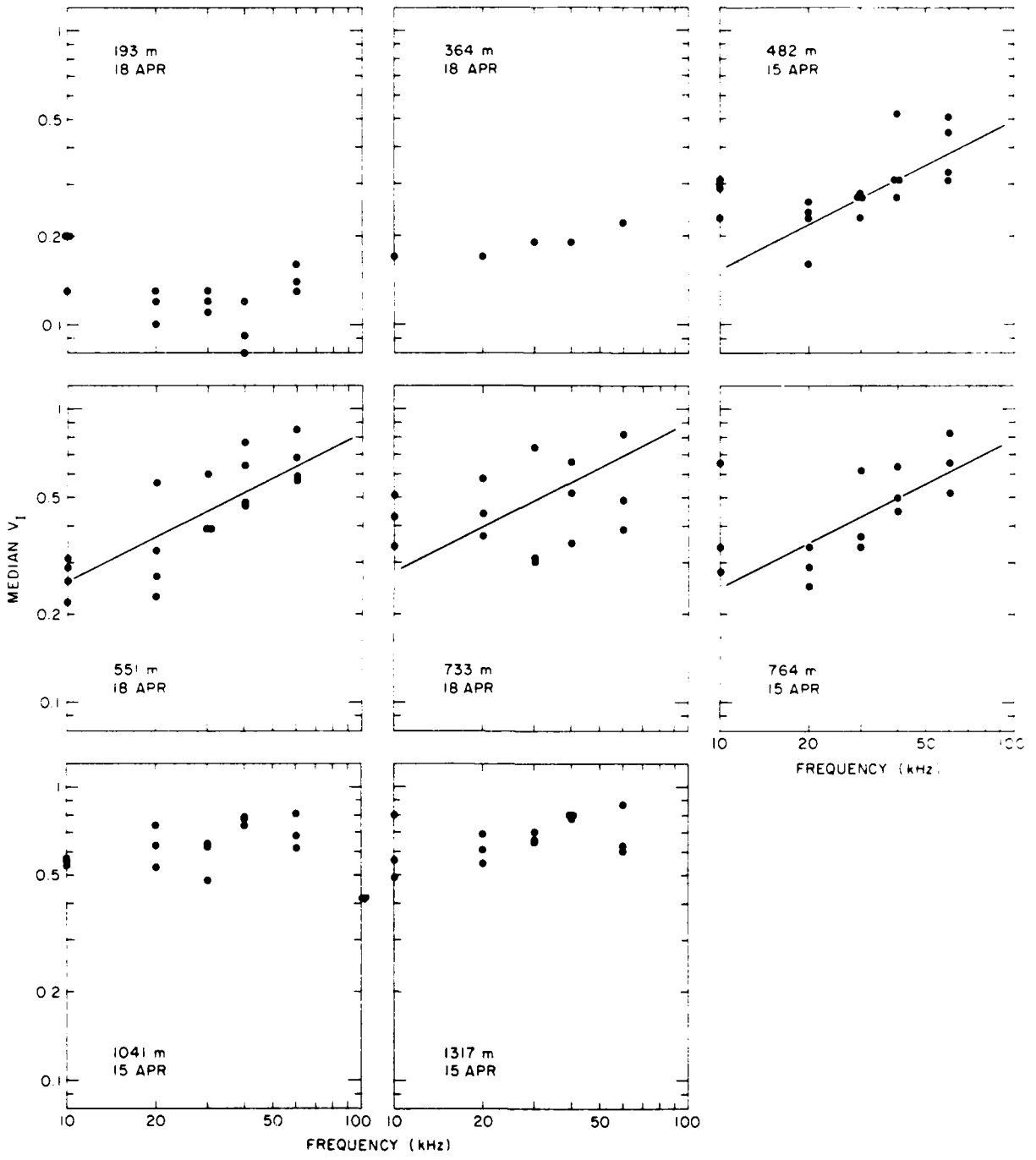

Figure 11. Coefficient of variation vs frequency for $|\theta| \geq 1.5°$ – Chukchi Sea (from Table A5). Lines are for $f^{1/2}$ dependence.

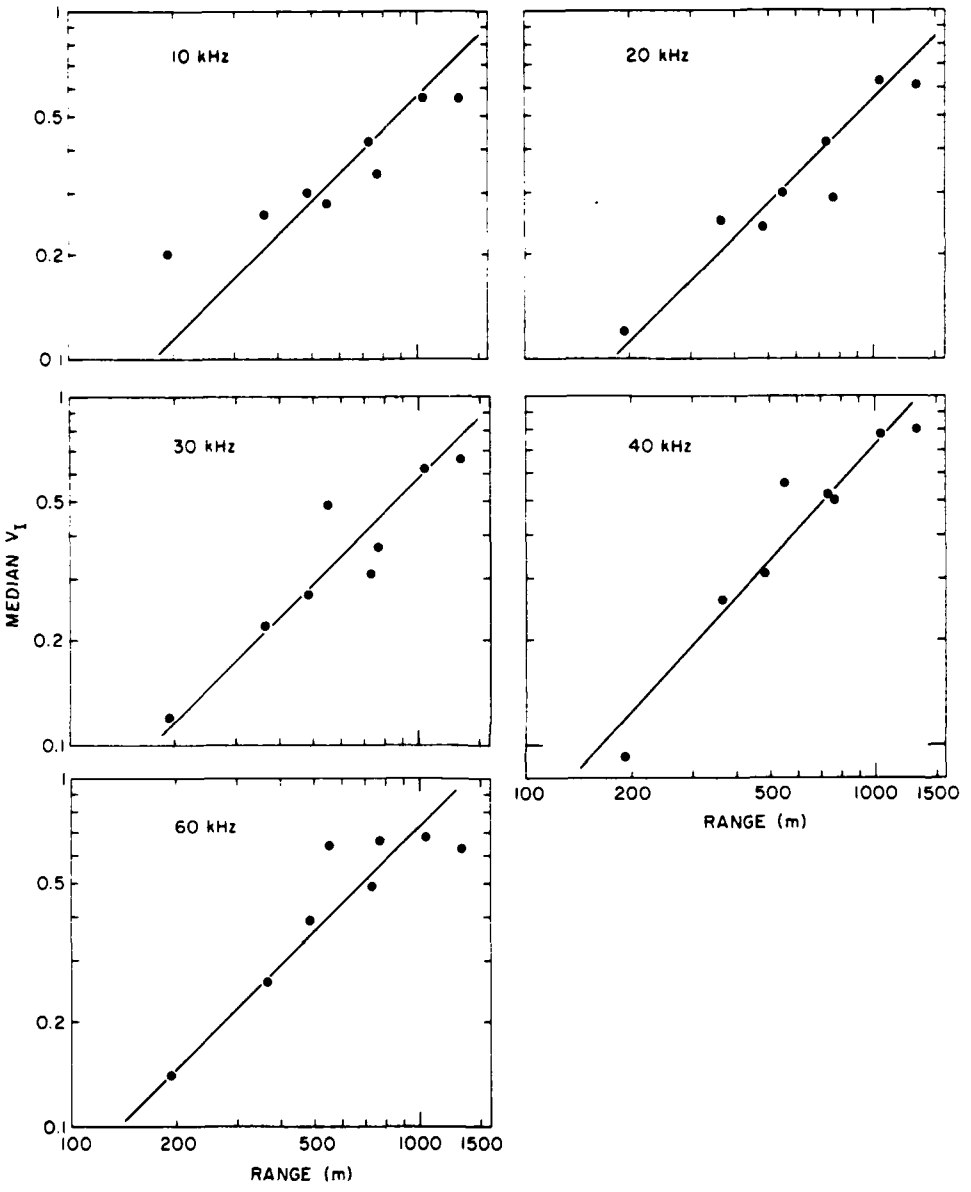

Figure 12. Coefficient of variation vs range for $|\theta| \geq 1.5°$ – Chukchi Sea (from Table A6). Lines are for $f^{1/2}$ dependence.

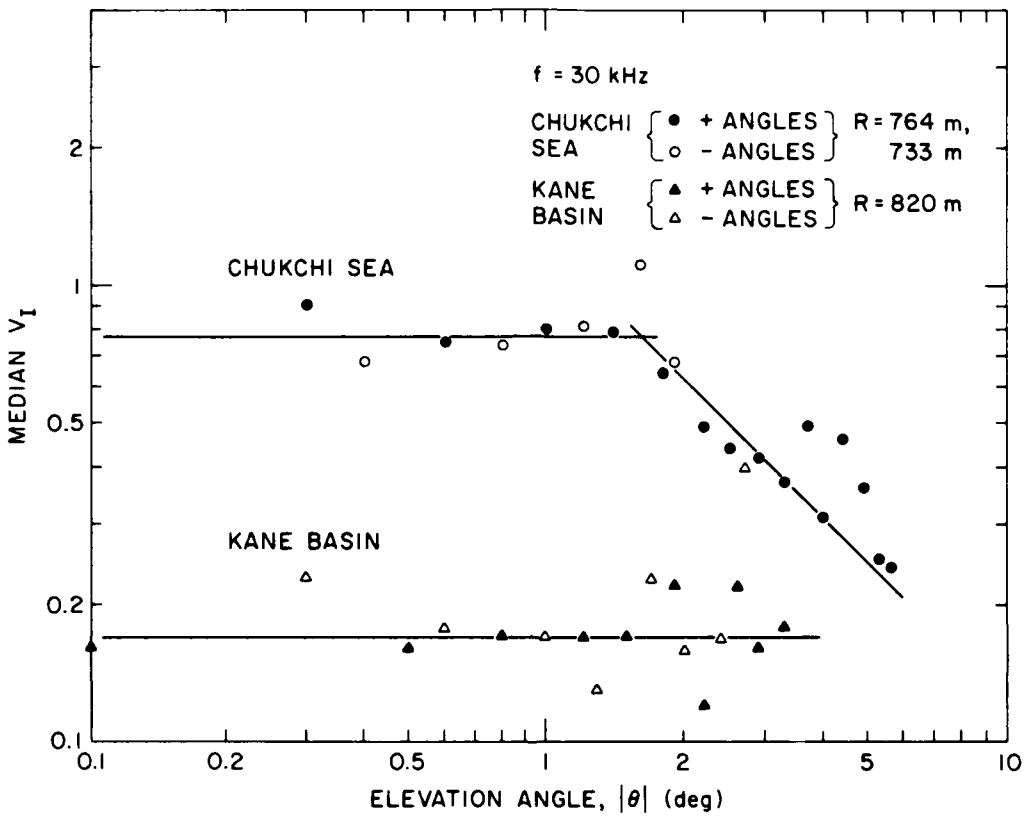

Figure 13. Typical dependence of coefficient of variation on elevation angle for Kane Basin and Chukchi Sea at a range near 800 m. Sloped line is drawn for $|\theta|^{-1}$ dependence. Tabulated V_I for various elevation angles are shown for the Chukchi Sea in Table A7.

Table 5. Limiting value of V_I at low angles, and cutoff angle — Chukchi Sea.

Range (m)	(kHz)	Upper V_I Limit	Magnitude of Cutoff Angle (deg)
482	10	0.44	2.40
	20	0.34	2.96
	30	0.45	2.55
	40	0.48	3.00
	60	0.58	3.10
550	10	0.70	1.58
	20	0.74	1.66
	30	0.81	2.08
	40	0.79	2.55
	60	0.90	2.25
733	10	0.67	2.03
	20	0.63	2.07
	30	0.74	1.75
	40	0.80	1.75
	60	0.84	2.35
764	10	0.65	1.32
	20	0.59	1.36
	30	0.80	1.46
	40	0.91	1.72
	60	0.89	1.54
1041	10	0.76	1.52
	20	1.01	1.35
	30	0.98	1.34
	40	0.92	1.85
	60	0.95	1.90
1317	10	0.79	1.01
	20	0.80	1.01
	30	0.95	0.84
	40	0.95	1.12
	60	0.83	1.20

The limiting value of V_I, as seen in Fig. 13 for the Chukchi Sea, is shown in Table 5 to be nearly independent of frequency. The range dependence is examined in Fig. 14 by plotting the median limiting values of V_I. For the ranges 193 m and 364 m, we have assumed that the values in Fig. 10 are the limiting values and have included their medians in the figure. The line represents a range dependence of $r^{3/2}$ for the near focusing region discussed in Ref. 13. The frequency independence observed in Table 5 also agrees with the characteristics discussed in that paper.

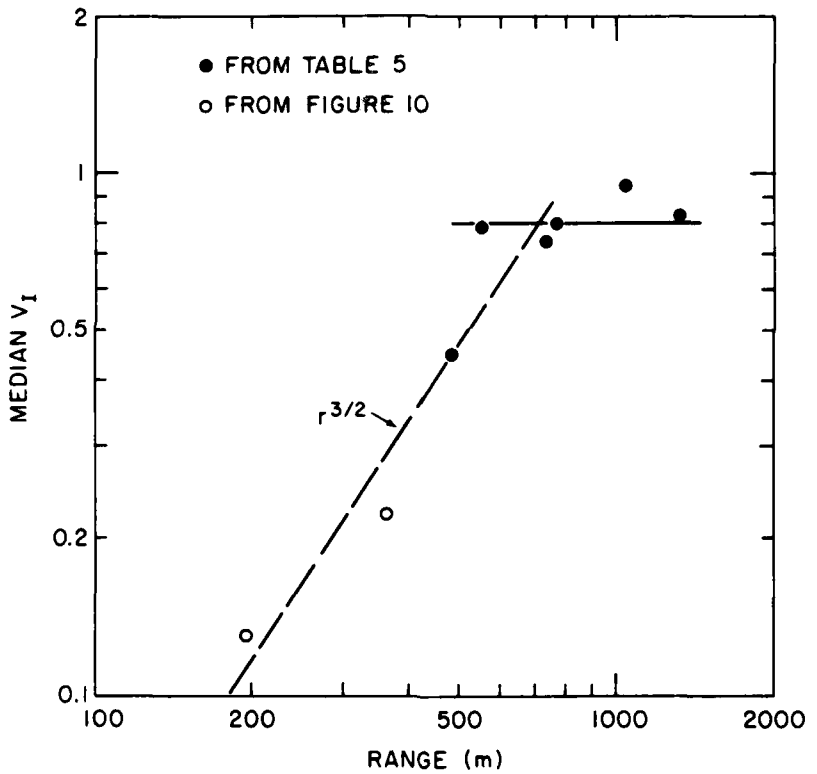

Figure 14. Limiting V_I level vs range for $|\theta| < 1.5°$ – Chukchi Sea. The dashed line represents the theoretical dependence, $r^{3/2}$.

III. AUTOCORRELATION FOR INTENSITY VS DEPTH

A. Introduction

The vertical-cast method of measuring intensity fluctuations allows determination of the vertical correlation length transverse to the propagation direction. In theories of propagation of sound waves through random media, the concept of correlation length relates the intensity variance to the refractive index variance. For anisotropic media, expressions have been developed that allow interpretation of the fluctuation data in terms of internal waves[6] or random Gaussian spheroidal inhomogeneities.[14,15] In the finestructure region of the spatial wavenumber spectrum, stratified elements can vary from highly anisotropic to isotropic, as the layers break down. We believe that vertical casts using several acoustic frequencies simultaneously furnish a potential method for determining the Ozmidov-Phillips, or buoyancy, scale. The buoyancy scale is a transition wavenumber at which the buoyancy subrange of ocean dynamics meets the isotropic inertial subrange.[12,16,17]

A previous paper[11] showed that large variability can arise from the interference between nearly horizontal rays transmitted close to a refracting layer. Expressions relating the intensity variance to the refractive index variance in the absence of extended layers are given in Ref. 13. To describe the scale of anisotropy detected by the use of a single acoustic frequency, vertical and horizontal correlation lengths are required. Further, to study the decay of eddies and layers toward isotropy, multifrequency and multirange data are required. Our experiments may provide these types of data if adequate space and time resolution is provided by the measurement technique. We also state again that the total variability is a combination of deterministic and statistical components.

B. Vertical Correlation Length

The concept of vertical correlation length involves changes in signal intensity in the vertical direction transverse to the propagation path. If the variation with time is slow enough, the vertical correlation length can be obtained from the autocorrelation in the received signals as the transmitting or receiving transducer is raised or lowered. The depth resolution for the intensity measurements was 0.10-0.40 m for the Kane Basin and 0.08 m for the Chukchi Sea. To eliminate the deterministic variations, the autocorrelations were computed on residuals from a 4-m running average of intensity. The choice of 4 m was somewhat arbitrary, but in our case this seemed to filter out the deterministic variations satisfactorily. As an example, Fig. 15 shows autocorrelograms of vertical intensity profiles in the Chukchi Sea at five frequen-

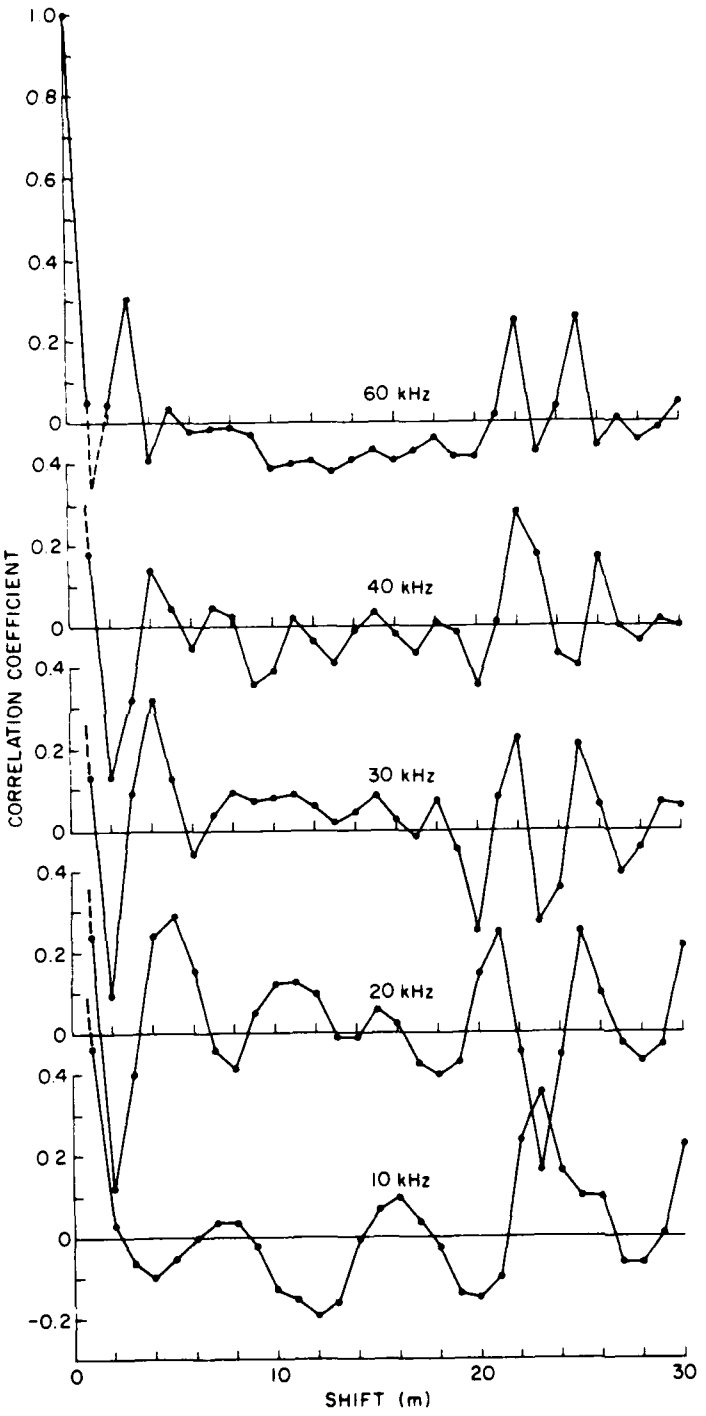

Figure 15.

Autocorrelation of vertical intensity profiles, computed on residuals from an average curve: range 482 m, transmitter at 70 m – Chukchi Sea.

cies. In this case, the residuals were from a curve of the variations common to all frequencies. The data points used for the correlation analysis were 1-m averages; thus the first zero-crossing is not accurately determined. In this case, the spacing of the correlation peaks is a measure of the correlation length. This spacing is seen in Fig. 15 to decrease as the acoustic frequency increases. Figure 16 shows auto-

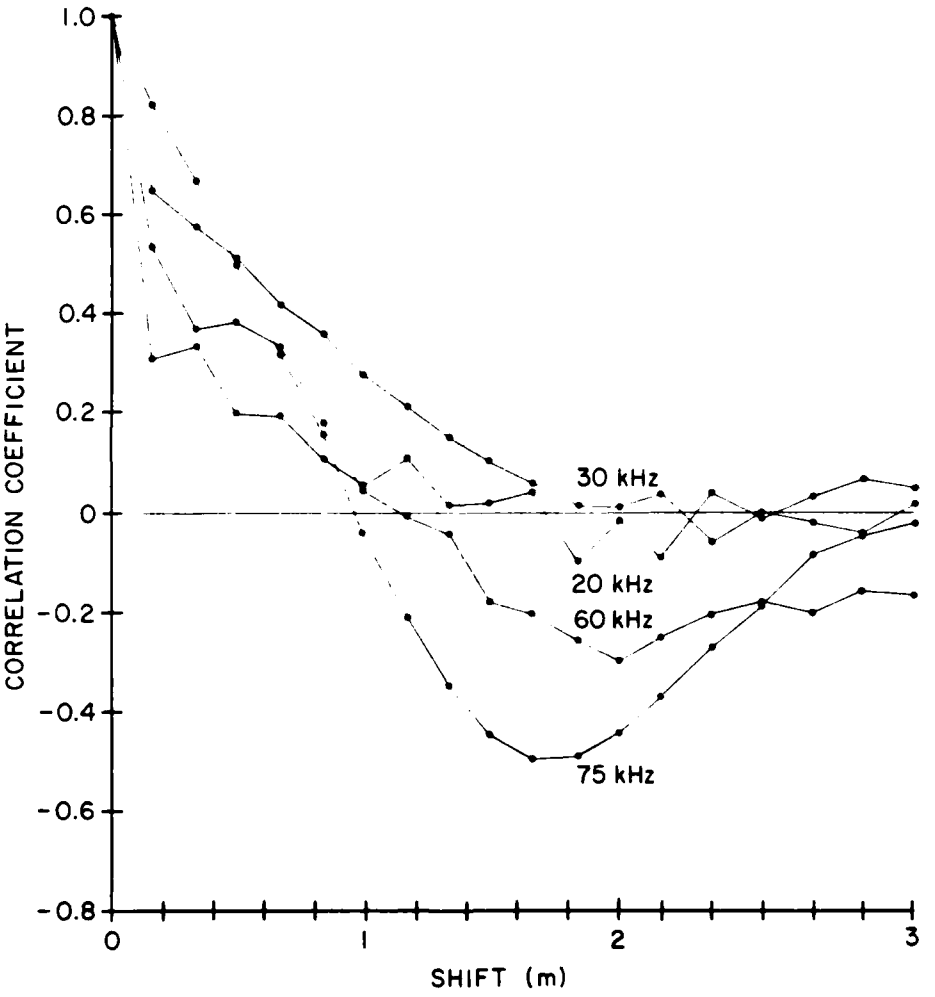

Figure 16. Autocorrelation of vertical intensity profiles, computed on residuals from smoothed data: range 1077 m, hydrophone 3 at 29 m, data set 1 – Kane Basin. The scale has been expanded to show the first axis crossing and the first minimum.

correlograms of vertical intensity profiles measured in the Kane Basin at four frequencies. The 10 kHz curve has been omitted because the plot was very erratic. Here, the data points were closely spaced, and consequently the zero crossing and first minimum are good measures of the correlation. These values tend to decrease with increasing frequency.

The value of the shift at the first minimum is taken as the "correlation length." In this sense, the correlation length corresponds to the vertical radius a_V of a Gaussian spheroid. Others[18] have used a similar procedure for horizontal measurements by running a projector-ship past a receiver-ship at various fixed ranges with the transducers of both ships at the same depth. The frequency was 25 kHz. The periodicity in the autocorrelation was taken as the "patch diameter" as we have done here.

C. Kane Basin

The median values obtained for the vertical correlation lengths in the Kane Basin are shown in Table 6. They appear to be independent of range and frequency, except for a tendency for the values to drop off at 75 kHz. The data are interpreted

Table 6. Vertical correlation lengths (m) — Kane Basin (computed on residuals from 4-m smoothed intensity-depth profiles; medians of five hydrophones, down and up casts).

Range (m)	Frequency (kHz) 10[a]	20	30	60	75	Median (m)
270	--	1.94	1.96	2.02	1.82	1.95
551	--	3.34	3.02	3.24	3.04	3.14
820	--	1.64	1.70	1.54	1.62	1.63
1077	--	1.78	1.82	1.74	1.56	1.76
Median (m)		1.86	1.89	1.88	1.72	1.87

[a] 10 kHz results were inconsistent, as seen in Figs. 7 and 8, and are omitted.

as due to isotropic patches with a radius of 1.9 m since the values cluster there for 20, 30, and 60 kHz. The correlation length a can be compared with a value calculated from theory[13] using measured values of V_I and the refractive index variance $\overline{\mu^2}$. However, because one of our objectives is to use acoustics to estimate oceanographic parameters, we will use the theoretical relationship to compute $\overline{\mu^2}$ from values of V_I and a and compare it with the value determined from CTD casts taken before and after the intensity measurements. This value was determined by calculating $\overline{\mu^2}$ for each interval as the mean square deviation of the refractive index μ about the least-squares line fitted to all values of μ in the interval.

To carry out this procedure we have assembled the median V_I data for the Kane Basin and plotted them in Fig. 17 against the scaled variable $k^{1/2}r$, where k is the acoustic wavenumber (m^{-1}) and r the range (m). In this report the spatial wavenumber is taken for convenience as the inverse of the wavelength, while the acoustic wavenumber retains its standard definition, 2π/wavelength.

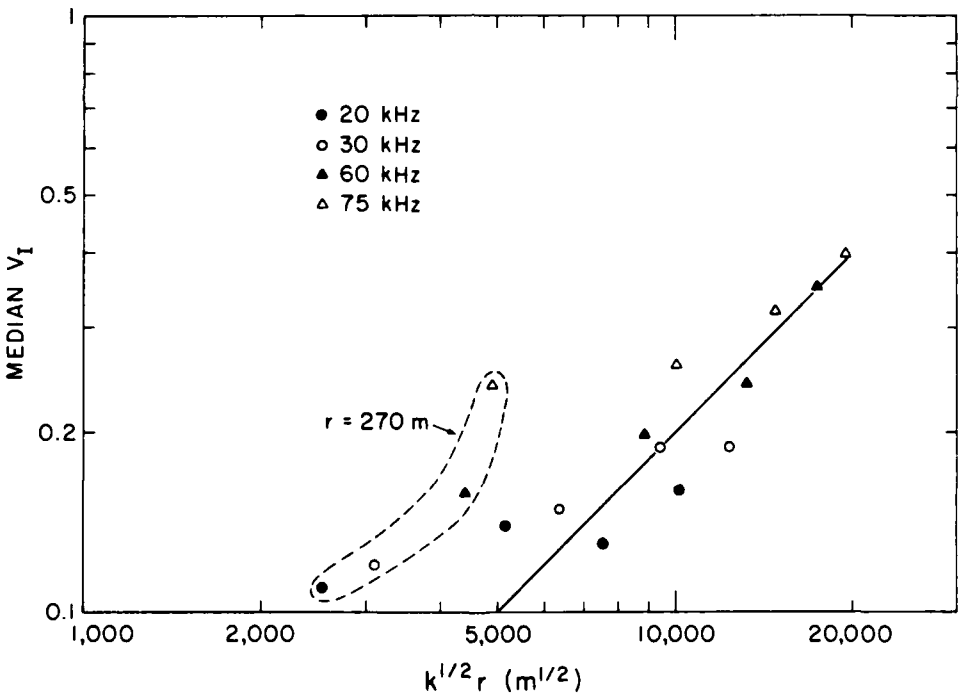

Figure 17. Coefficient of variation scaled to $k^{1/2}r$, where k is the acoustic wavenumber (2π/wavelength) and r is the range – Kane Basin.

We see that the plot is independent of frequency, supporting the quasi-isotropic model for the scattering. The four points at the left that seem to be out of line are for the shortest range, 270 m. The data are expected to follow the solution given by Eq. 9 in Ref. 13 to the isotropic formula for the middle region:

$$\overline{V_l^2} = 1.12 \frac{\overline{\mu^2}}{a} k r^2 \qquad (1)$$

for $0.59 \leq x \leq 3.16$, where x is r/ka^2. Since a was found to be about 1.9 m (Table 6), the computed value of $\overline{\mu^2}$ is 0.7×10^{-9}. This value is in agreement with estimates obtained in other ways, as shown in Section IV. It should be mentioned that the values measured for a satisfy the required bounds of the middle region.

D. Chukchi Sea

The median values found for the vertical correlation lengths in the Chukchi Sea are plotted in Fig. 18. As for the Kane Basin, they are nearly independent of range. In the plot, the vertical correlation length is observed to fall off as the square root of frequency, whereas the vertical correlation lengths for the Kane Basin (Table 6) seemed to have only a slight decrease with frequency in the frequency range used.

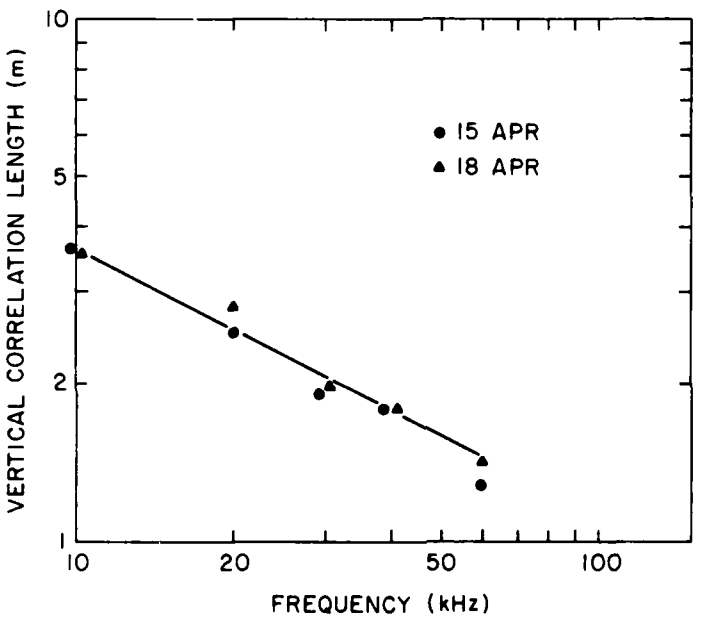

Figure 18. Vertical correlation length vs frequency – Chukchi Sea, all ranges. The line represents an $f^{1/2}$ dependence. The correlation lengths for individual runs are shown in Table A8.

In relating the vertical correlation lengths in the Chukchi Sea to the variance at each frequency, the full anisotropic expression for the middle region (Ref. 13, Eq. 26) is used:

$$\overline{V_I^2} = 0.607\overline{\mu^2}\,\frac{a_H}{a_V^2}(\nu+0.855)\,k\,r^2\,, \tag{2}$$

where a_H is the horizontal correlation radius of the nonisotropic inhomogeneities, $\overline{\mu^2}$ is the refractive index variance, and $\nu=(a_V/a_H)^2$. The region boundaries are, with $x_V = r/(k\,a_V^2)$,

$$\frac{0.856(\nu+0.855)}{(\nu^2+\frac{2}{3}\nu+1)} \leqq x_V \leqq \frac{5.83}{(\nu+0.55)}\,.$$

We must now use measured values for the parameters V_I, $\overline{\mu^2}$, and a_V to find $\nu^{1/2}$ and consequently a_H. For this purpose, Eq. 2 is written with a_H eliminated so that $\nu^{1/2}$ can be computed in terms of a_V:

$$\overline{V_I^2} = 0.607\,\frac{\overline{\mu^2}}{a_V}\left[\nu^{1/2}+\frac{0.855}{\nu^{1/2}}\right]k\,r^2\,. \tag{3}$$

The data used and the calculated values of $\nu^{1/2}$ and the corresponding a_H are shown in Table 7. The value $\overline{\mu^2} = 2.27\times10^{-9}$, derived later in Section IV, was used for these calculations.

Table 7. Calculation of the anisotropic ratio a_V/a_H *and thereby the horizontal correlation length* a_H*, as detected at each frequency — Chukchi Sea, 1974.*

	Frequency (kHz)				
Parameter	10	20	30	40	60
a_V (m)	3.58	2.66	1.96	1.80	1.36
k (m^{-1})	43.7	87.4	131	175	262
V_I^2	0.06	0.12	0.19	0.25	0.37
a_V/a_H or $\nu^{1/2}$	0.14	0.19	0.27	0.30	0.44
a_H (m)	25.0	14.0	7.3	6.1	3.1

The calculation was made at a range of 764 m for which V_I was interpolated in Fig. 12 and fitted to an $f^{1/2}$ dependence.

The dependence on acoustic frequency of the correlation structures found in the Chukchi Sea measurements allows us to estimate by extrapolation the Ozmidov-Phillips transition scale from the anisotropic buoyancy subrange to the isotropic inertial subrange, as shown in Fig. 19. At higher frequencies the correlation radius has been found[19] to continue to decrease to a limiting value of 1 cm for water.

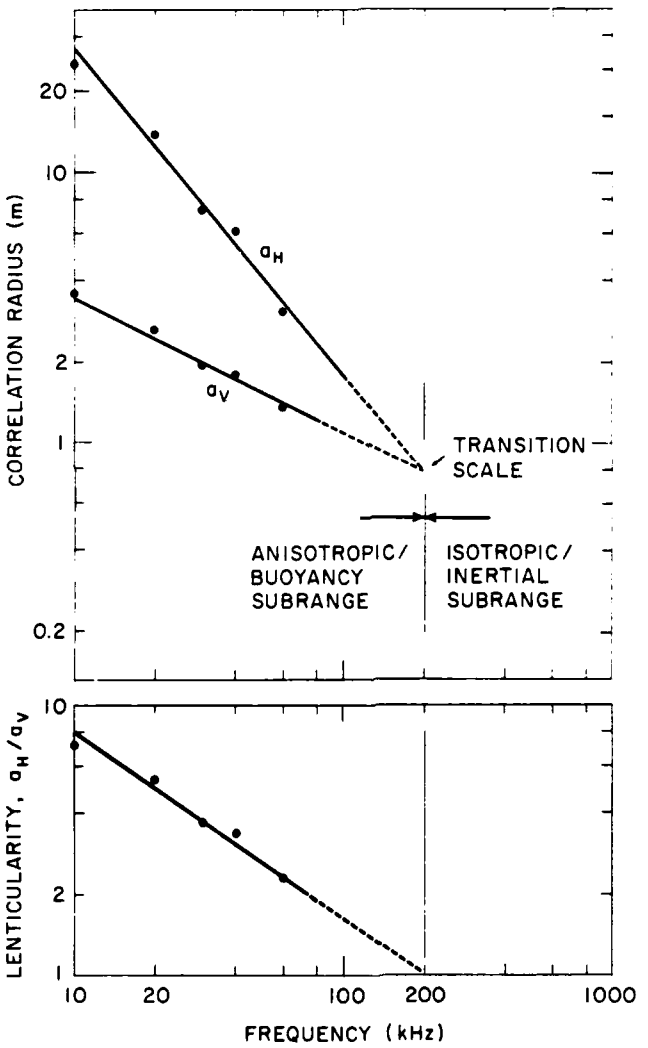

Figure 19. Values of a_V and a_H detected at different acoustic frequencies – Chukchi Sea (from Table 7). A lenticularity of 1 means isotropy.

E. Properties of Scattering Patches

The results for the anisotropic ratios are quite unexpected and require discussion. The low ratios indicate a dynamic situation, involving eddies or circulating current cells. Such cells are close to being isotropic and could be part of the eddy cascade to smaller scales of the inertial subrange. We know that their lifetime exceeds the few seconds involved in taking data over the vertical correlation length. These cells or eddies must exist in nearly statistical equilibrium, with as many being generated as are decaying. Under the conditions of the arctic experiments, one of the energy sources creating them could be the shear caused by the effect of ice floe motion on the layered density gradients of the near-surface halocline and deeper thermocline.[20]

It is also of interest to compare our autocorrelation results with the results of acoustical determinations in other oceans (Table 8). These comparisons are made at 25 kHz because there are a number of measurements reported in the literature at this frequency[18,21,22] . The value found was assumed to be a_V. As can be seen in Table 8, the measured values of a_V are in line with correlation structures found elsewhere in the world. The lenticularity (a_H/a_V) of 4 found by Whitmarsh *et al.*[18] is in agreement with the line plotted in Fig. 19 for the Chukchi Sea (i.e., 4.3 at 25 kHz).

Table 8. Comparison with correlation radii, a, obtained by other investigators, at f = 25 kHz.

Location/Date	a (m)	Reference
Chukchi Sea (April 1974)	2.3	Present (a_V)
Kane Basin (April 1979)	1.9	Present (a_V)
Key West (January 1957)	2.5	18
Key West (March 1957)	2.4	18
Key West (July 1957)	1.7	18
North Atlantic (May 1961)	~1.4	20
Northwest Atlantic (May 1962)	~0.4	21
Northeast Atlantic (June 1962)	~1.6	21
Sea of Norway (July 1962)	~0.7	21

F. Plots with Scaled Parameters

It has become customary to plot the results of acoustic scattering experiments in a plane with a strength parameter as the ordinate and a diffraction or wave parameter as the abscissa, since such plots enable comparison of measurements at different depths, ranges, and acoustic frequencies. At least two sets of scales are popular: the $\Phi\Lambda$ scale of Flatté et al.[6] and the ΓX scale of Uscinski.[7,8]

In the Flatté *et al.* plot, the strength parameter Φ is the rms phase fluctuation over the acoustic path in the direct-path regime,

$$\Phi = [k^2 \overline{\mu^2} a_H r]^{1/2} ,$$

and the diffraction, or wave, parameter Λ is the range scaled to the average Fresnel zone radius,

$$\Lambda = r/(6k\, a_V^2) ,$$

where k is the acoustic wavenumber, $\overline{\mu^2}$ is the mean-square space-time refractive index over the vertical correlation length a_V, and r is the range. The horizontal correlation length a_H is taken here as the correlation length along the nearly horizontal path.

Equivalently, in Uscinski theory, the strength parameter Γ is the phase variance per unit scaled range (Φ^2/X) in the direct-path region,

$$\Gamma = \overline{\mu^2}\, a_H a_V^2 k^3 ,$$

where X is the scaled range,

$$X = \frac{r}{k\, a_V^2} .$$

In Fig. 20, the areas bounding the results are shown in the $\Phi\Lambda$ plane for both experiments. All the results lie in the unsaturated direct-path region as they should. In Figs. 21a,b the scattering results for direct-path propagation are shown for the ΓX plane. Again, both the Kane Basin data and the Chukchi Sea data are well within the unsaturated region.

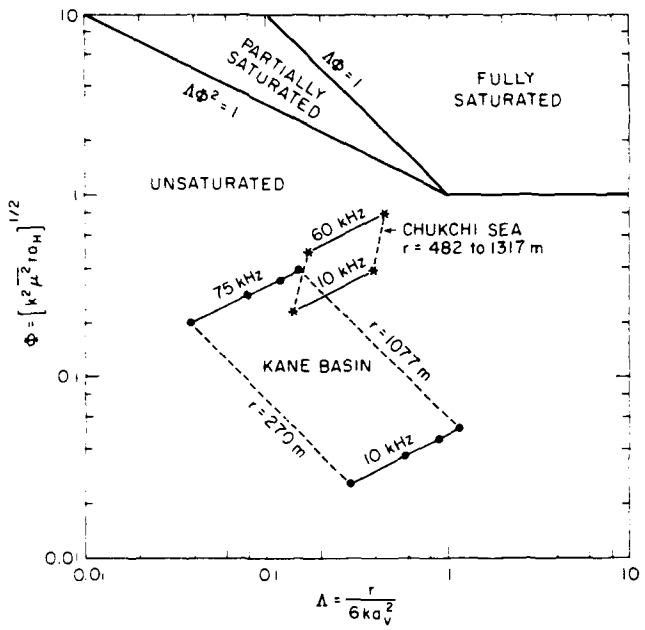

Figure 20.

ΦΛ plane for both locations. The bounds of each set of measurements are shown.

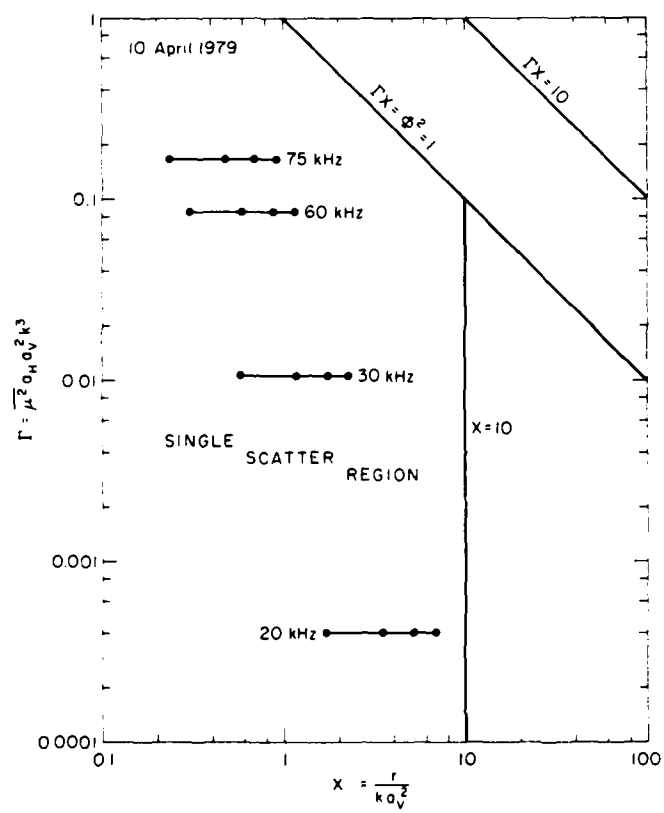

Figure 21a.

ΓX plane (after Uscinski) for Kane Basin measurements.

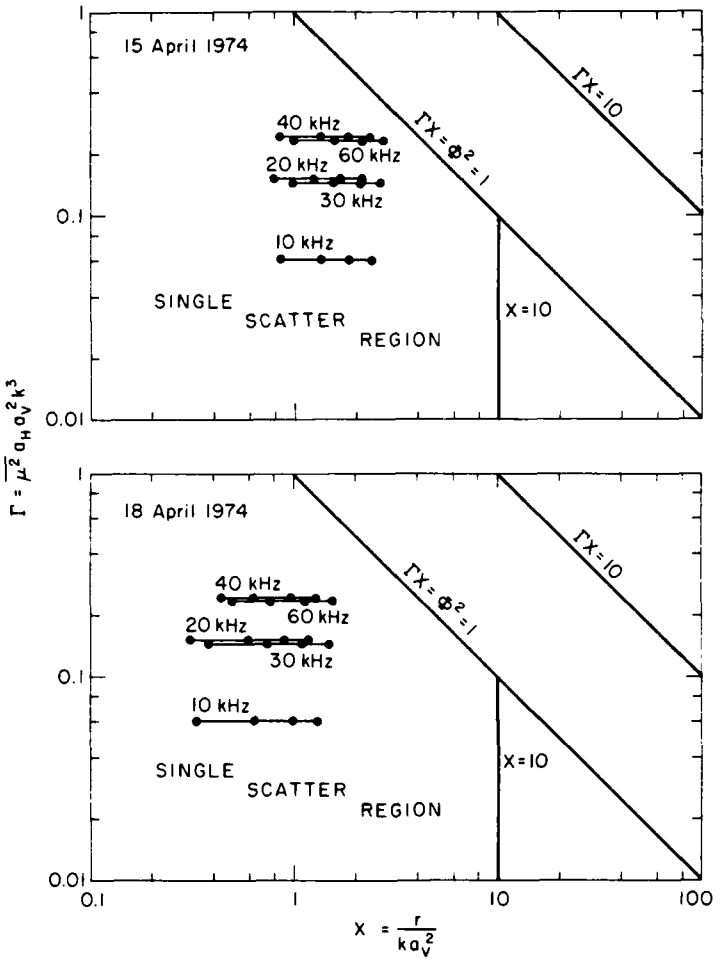

Figure 21b. ΓX plane for Chukchi Sea measurements, 15 and 18 April 1974.

G. Spectra of Intensity Variation with Depth

The spectra of the 4-m smoothed vertical intensity profiles taken in Kane Basin at a range of 820 m are plotted in Fig. 22 for all five frequencies. A line with variance $\sim K^{-5/2}$ (K is the vertical spatial wavenumber) represents anisotropic inhomogeneities. A $K^{-5/3}$ line would represent isotropic conditions. The data at the five acoustic frequencies do not follow either law well enough to indicate which law applies. The initial smoothing to remove the deterministic component may have reduced the variance at the lower spatial frequencies for the remaining random variations.

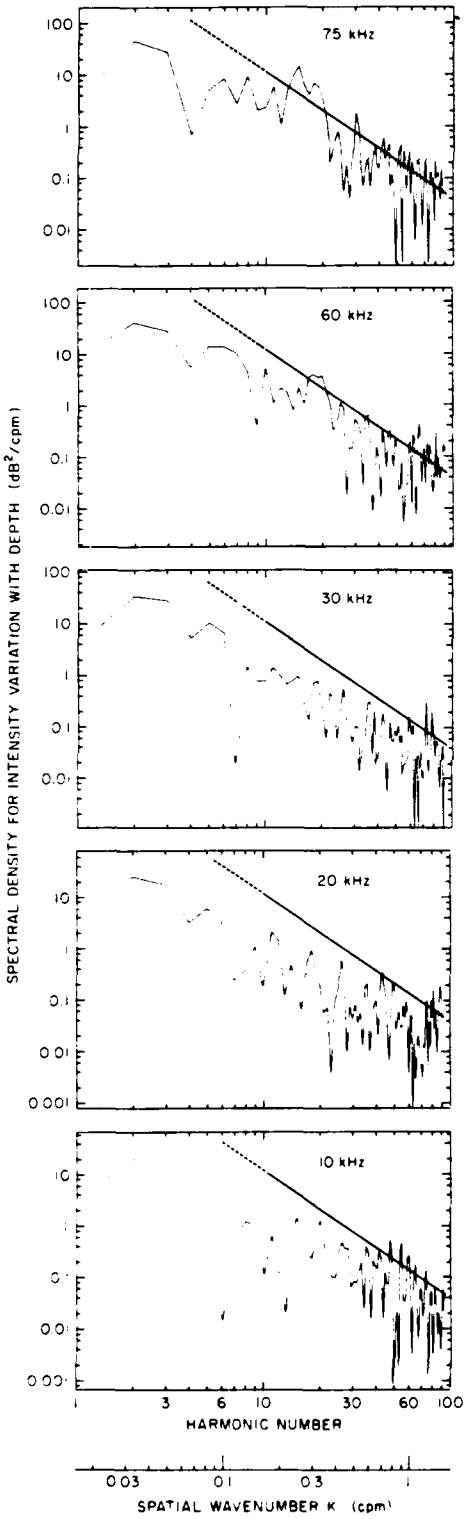

Figure 22.

Power spectrum of intensity; r = 820 m, Kane Basin. A Hanning window was applied to the data in the 10-70 m depth interval. The first harmonic corresponds to a wavelength of 60 m. A line with a slope of -5/2 has been drawn at the same density level in all graphs.

IV. REFRACTIVE INDEX VARIANCE

In general, theory requires that the variance of acoustic intensity be proportional to the variance of sound speed along the ray path. Time variations in the refractive index were not measured separately in our studies. Although other workers have found that, at 25 kHz in the open ocean, the pertinent refractive index inhomogeneities[18,22] have time durations of about 1 to 3 s, conditions in the Arctic are more stable. Our estimate of the sound speed variance for the present study comes mainly from the measurements of temperature and salinity vs depth that were obtained before and after the acoustic runs. The vertical resolution of these measurements was 0.3 to 0.4 m, which corresponds to the sampling interval of 0.5 s. The variability in sound speed along the path is expected to result from variations in three components – temperature, salinity, and current. As a practical measure, we have used the variance in sound speed at one location, over the depth interval occupied by the contributing ray paths. Fluctuations in current have been neglected in this study even though their effect can be sizable. They should be considered in future field measurements.

The equations[13] that are used to relate the intensity variance to the refractive index variance have been derived based on the time variability of the transmission between two fixed points. Our measurements were made with the source or receiver moving, and thus we measured variations in space-time which we consider an upper limit to the single-path time variations. In our analysis we used the variations within small (5 m) intervals as a means of obtaining a reasonable estimate of the time variations treated by the theory.

A. Dependence on Depth Interval Size

To obtain the small-scale fluctuations about the local refractive index gradient, $\overline{\mu^2}$ values were calculated for various depth intervals from 5 to 60 m in length. This was done by fitting the refractive index data for each interval with the best straight line and taking the mean square deviation from the line as $\overline{\mu^2}$. Correlation lengths were calculated for each interval. The dependence of $\overline{\mu^2}$ and the correlation length on interval size is shown in Figs. 23-25. A depth interval of 5 m is the smallest possible division for which $\overline{\mu^2}$ can be calculated with a reasonable statistical accuracy. A depth interval of 5 m corresponds to a time interval of about 5 s. By eliminating the effects of the local vertical temperature and salinity gradients, we obtain a $\overline{\mu^2}$ representative of finestructure and other small-scale processes.

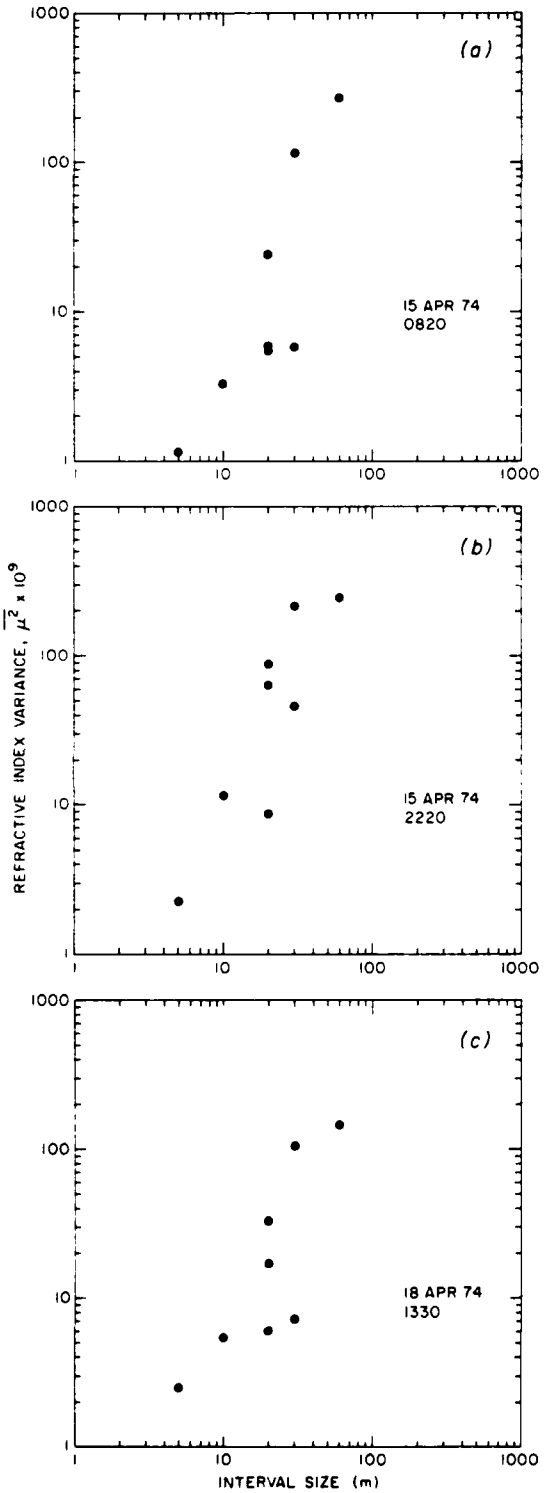

Figure 23.

Refractive index variance $\overline{\mu^2}$ vs depth interval – Chukchi Sea. Values of $\overline{\mu^2}$ are listed in Table A9 for various depth intervals for these three runs in April 1974.

Figure 24.

Refractive index variance $\overline{\mu^2}$ vs depth interval – Kane Basin. Values of $\overline{\mu^2}$ are listed in Table A9 for various depth intervals for these two runs on 10 April 1979.

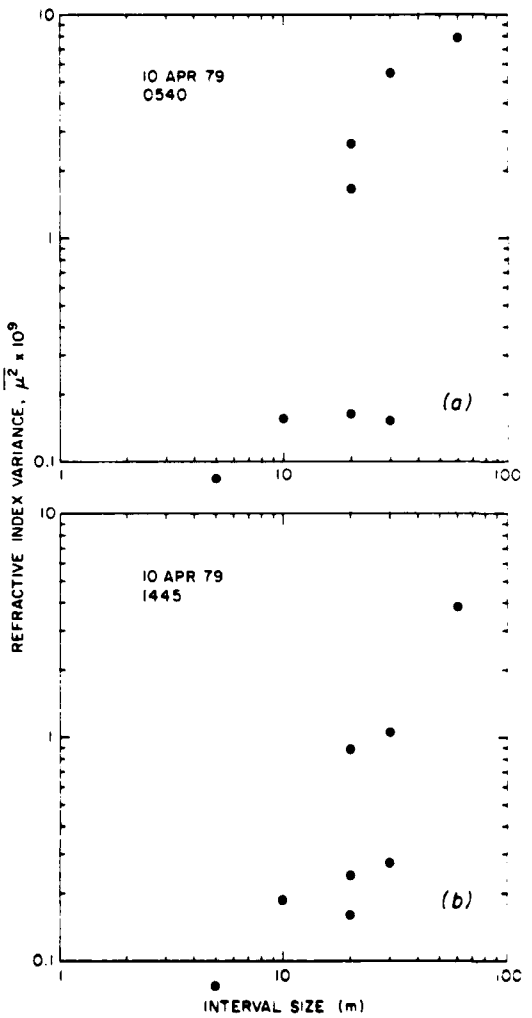

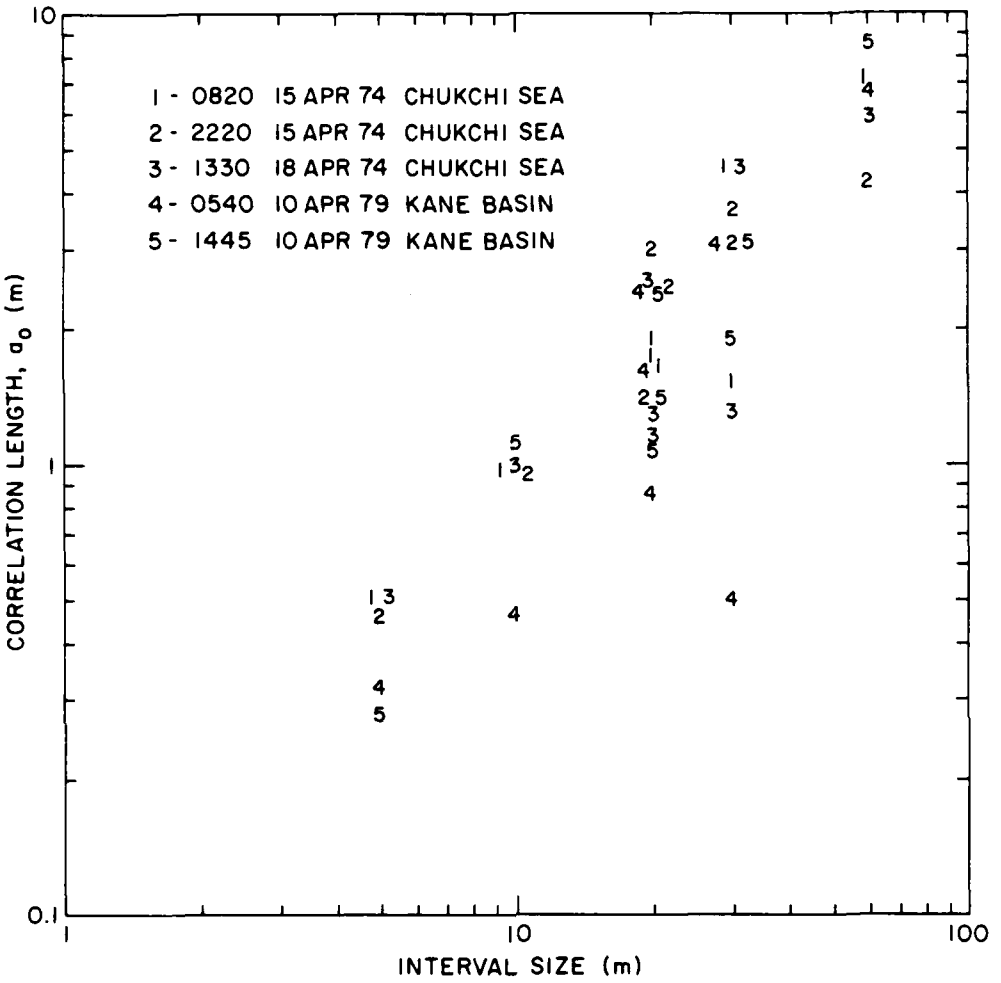

Figure 25. Correlation length for refractive index – both locations (Table A9).

The results in Figs. 23-25 were useful for relating acoustic and refractive index variations (Section III), and the values of $\overline{\mu^2}$ will now be compared with those produced by internal waves.

B. Relation to Internal Waves

In calculating the refractive index variance $\overline{\mu^2}$ due to internal waves, we assume that oscillations of the internal waves and finestructure layers follow the equation[6]:

$$\overline{\mu^2} = \langle\zeta^2\rangle\left[\frac{1}{C}\frac{\partial C_p}{\partial z}\right]^2 \qquad \text{(1.6.8 in Ref. 6)}$$

and that

$$\frac{1}{C}\frac{\partial C_p}{\partial z} = G(z)n^2(z)\,, \qquad \text{(1.1.9 in Ref. 6)}$$

where $\langle\zeta^2\rangle$ is the time average of the square of the displacement, C is the sound speed, $\partial C_p/\partial z$ is the potential sound speed vertical gradient, and n is the buoyancy frequency. G relates the potential sound speed to the buoyancy frequency and is highly variable in the surface layers of the Arctic.

For internal waves $\langle\zeta^2\rangle \sim 1/n$, so that, if $\langle\zeta_0^2\rangle$ and n_0 are known for some reference point 0, $\langle\zeta^2\rangle n = \langle\zeta_0^2\rangle n_0$, and

$$\overline{\mu^2} = \langle\zeta_0^2\rangle G^2 n_0 n^3\,. \qquad \text{(1.6.9 in Ref. 6)}$$

In the Chukchi Sea the surface activity generally occurs above the halocline which is at about 30 m depth. Below the halocline conditions are more stable and the density gradient is fairly constant. In the 40-70 m region the internal wave frequency is sufficiently constant that we would expect to find refractive index variations related to that particular frequency. We proceed now to compare the $\overline{\mu^2}$ values for the 40-70 m depth interval in Figs. 23 and 24 for both locations with the values predicted for internal waves.

For the data taken in the Chukchi Sea at 0820 on 15 April 1974, the buoyancy frequency is calculated to be 6.0 cph and $\frac{1}{C}\frac{\partial C_p}{\partial z} = 8.73 \times 10^{-4}\ \mathrm{m^{-1}}$. Thus, $G = \frac{1}{n^2}\left[\frac{1}{C}\frac{\partial C_p}{\partial z}\right] = 0.22\ \mathrm{m^{-1}\,s^2}$. For a representative value of the product $\langle\zeta_0^2\rangle n_0$, we use values measured at 48 m depth in the Chukchi Sea in October 1982: $n_0 = 6.7$ cph and $\langle\zeta_0^2\rangle = (2.8)^2 = 7.8\ \mathrm{m^2}$ with a product of $0.091\ \mathrm{m^2\,s^{-1}}$. Finally, we have from the last equation above for $\overline{\mu^2}$:

$$\overline{\mu^2} = 4.4 \times 10^{-3} n^3\,,$$

$$= 5.1 \times 10^{-9}\,.$$

This estimate compares well with $\overline{\mu^2} = 5.8 \times 10^{-9}$ shown in Fig. 23a (the smaller 30 m value is for the 40-70 m depth interval).

In the Kane Basin, water properties were nearly constant. Here again, the 40-70 m depth interval was the most uniform, with constant salinity and a small increase in temperature with depth. For the CTD measurement at 1445 on 10 April 1979, the potential density gradient was 0.17×10^{-6}. The corresponding internal wave period is 0.73 cph, and the temperature gradient gives $G = 6.9\ m^{-1}\ s^{-2}$. If we assume the internal wave amplitude was the same as for the two-cycle measurement in October 1982 in the Chukchi Sea, we obtain $\overline{\mu^2} = 1.0 \times 10^{-9}$, which is in close agreement with the measured value of 1.04×10^{-9} shown in Fig. 24b (the larger 30 m value is for the 40-70 m interval).

The agreement in the 40-70 m interval between the measured variation in the refractive index and that predicted from internal waves indicates that these relatively high-frequency internal waves are a likely cause of the variations and the resulting acoustic fluctuations. The variability closer to the surface seems to be complicated by complex energy interchanges.

C. Spectral Analysis

Vertical spectra of the spatial wavenumbers were calculated for the refractive index profiles obtained from the CTD data for both Kane Basin and the Chukchi Sea. In calculating these spectra, a Hanning window was applied to the 10-70 m data for both locations. The results are shown in Fig. 26; the same $K^{-5/2}$ line has been drawn in each graph for reference. For spatial wavenumbers of 0.1-1.0 cpm, the falloff is fairly consistent, but with a smaller slope, more like K^{-2}.

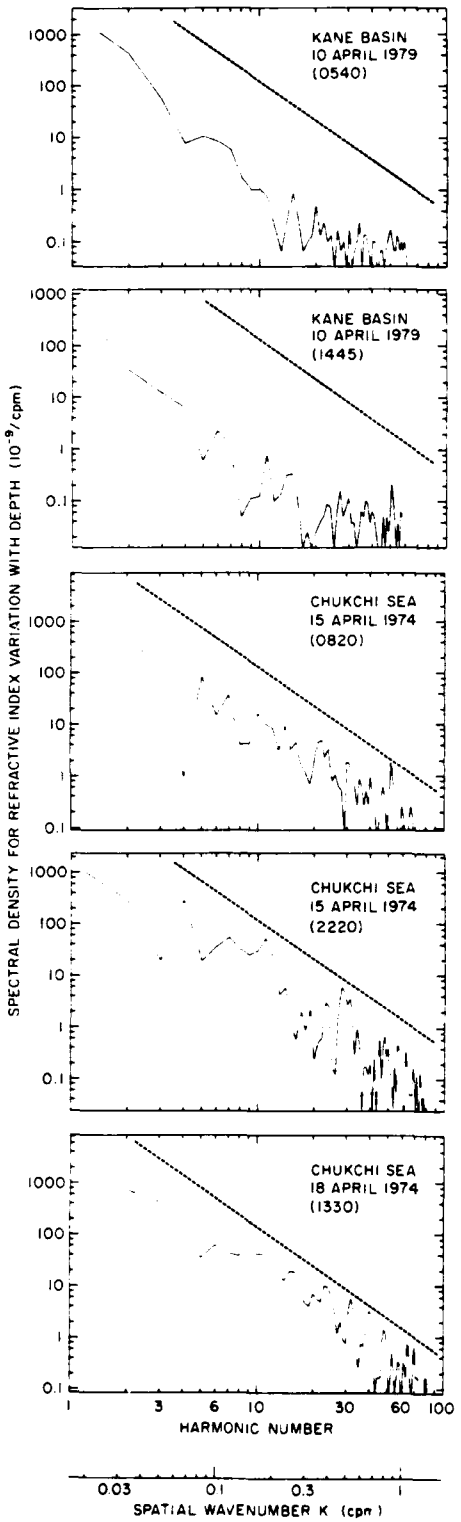

Figure 26.

Power spectrum of refractive index. A Hanning window was applied to the 10-70 m data at both locations. The first harmonic corresponds to a wavelength of 60 m. A line with a slope of -5/2 has been drawn at the same density level in all graphs.

V. SPATIAL CORRELATION OF THE INTENSITY – KANE BASIN

The inhomogeneities associated with oceanic finestructure and turbulence reduce the correlation of signal fluctuations both along and transverse to the propagation path. Because we used an array of five hydrophones spaced perpendicular to the transmission path, we were able to test the scale of intensity coherence in the Kane Basin measurements by computing the cross correlation between the intensities at the different hydrophones.

A. Transverse Horizontal Correlation

The transverse horizontal correlation was computed for intensity measurements at each of the four ranges in the Kane Basin experiment. For these calculations, we used the three hydrophones that were spaced at 30, 60, and 90 m along a horizontal line perpendicular to the propagation path. Prior to the correlation analysis, the intensity data (set 1 for depths of 20-70 m) were smoothed by taking a 4-m running average. The cross correlations were computed for various transverse horizontal spacings of the hydrophones. The correlations for up-casts were computed separately from those for down-casts. In Table 9a, the median correlation coefficient at each spacing and frequency is shown for all ranges.

An analysis of the range dependence of the transverse horizontal correlations showed that for direct-path propagation the correlation coefficient ρ is related solely to the horizontal angle φ subtended at the source by $\rho = e^{-q\varphi}$. To examine the frequency dependence, q was computed for each value of ρ that contributed to Table 9. These values of q were then averaged for each frequency and plotted with error bars in Fig. 27. The best fit for the dependence of q on the frequency f in kilohertz is given by

$$q = 0.80 f^{0.51 \pm 0.06}. \tag{4}$$

If frequency is converted to wavelength using $f = C/\lambda$, where $C = 1.44 \times 10^3$ m s^{-1},

$$q = (0.92/\lambda)^{1/2}.$$

The constant 0.92 must have units of length and can be considered as a "characteristic length" for the correlation.

Table 9. Correlation between intensity profiles for pairs of hydrophones. The profiles from 20 to 70 m were first smoothed by taking a 4-m running average.

(a) Horizontally spaced hydrophones (see Table A10 for the correlation for each pair of runs).

Medians for All Ranges

Spacing (m)	Frequency (kHz) 10	20	30	60	75
30	0.95	0.82	0.81	0.69	0.59
60	0.77	0.61	0.56	0.64	0.51
90	0.84	0.59	0.60	0.56	0.51

(b) Vertically spaced hydrophones (see Table A11 for the correlation for each pair of runs).

Medians for All Ranges

Spacing (m)	Frequency (kHz) 10	20	30	60	75
10	0.20	0.17	0.20	0.26	0.13
20	0.20	-0.10	0.09	0.08	0.20
30	-0.10	-0.20	-0.44	-0.25	0.05

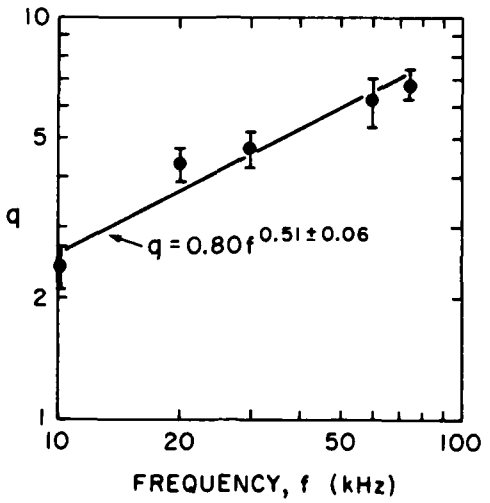

Figure 27.

Transverse horizontal correlation parameter q vs frequency f.

B. Transverse Vertical Correlation

Using 4-m running averages of the data, we computed the cross correlations of the intensities at the three hydrophones, which were spaced in a vertical line 10, 20, and 30 m apart. The results are shown in Table 9b. Note that the correlation is very low, in many cases too low to be significant. Thus a closer spacing is required, which was achieved with a continuous vertical drop (Section III).

C. Correlation Between Frequencies

Taking the data at several frequencies simultaneously allows an accurate determination of the correlation between the intensities at the different frequencies. Fig. 28 is a plot of the median correlation coefficient ρ as a function of frequency ratio F for pairs of data sets at the five frequencies. The values for each range are the medians for the data from all five hydrophones. The correlation is high at all three ranges. In Fig. 28, a dependence given by $\rho = F^{-1/4}$ (for $F>1$) gives the trend of the data.

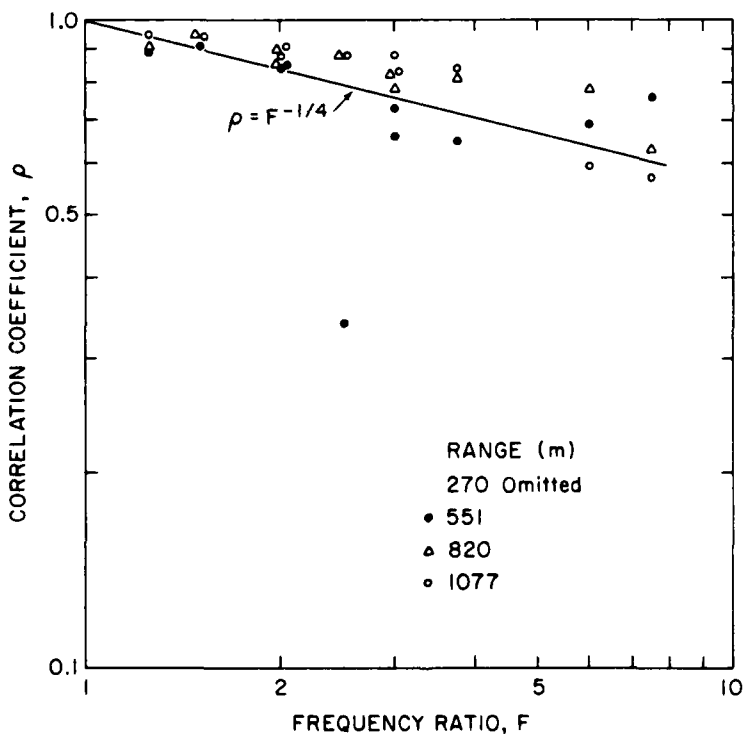

Figure 28. Correlation coefficient vs frequency ratio – Kane Basin.

VI. CONCLUSIONS

Sound propagation fluctuations were measured at two locations in the Arctic with widely different refractive index variability – the nearly homogeneous waters of the partially enclosed Kane Basin and the intrusively layered waters of the Chukchi Sea. Analysis of intensity variations with depth reveals that the acoustic characteristics of the medium can be determined from measurements at several frequencies simultaneously. These acoustic characteristics can be related to the vertical temperature and salinity profiles. The results indicate that for vertical profiles of the intensity a vertical resolution of 0.1 m is desirable for frequencies of 10-75 kHz.

In analyzing the data, the acoustic intensity variance, the vertical correlation length, and the coherence were computed for the small-scale spatial variations and found to have the following properties:

(1) *Variance.* In both locations the variance V_f^2 at frequency f and range r follows the law

$$V_f^2 \sim f\, r^2.$$

In the Chukchi Sea, a limiting value in the variance was observed as the ray elevation angle decreased below 1.5°. This limiting value can be appreciably less than unity and is nearly independent of frequency. It is thought to result from focusing and ducting by finestructure layers. For small elevation angles greater than 1.5°, the variance falls off as the square of the elevation angle. In the Kane Basin no limiting value was found at low angles.

(2) *Autocorrelation.* Analysis of Chukchi Sea data taken at several frequencies simultaneously provides vertical correlation lengths at these frequencies. Equations developed in an earlier paper were used to compute the corresponding horizontal correlation lengths. As the acoustic frequency increases, the apparent scale of the scattering structures changes, causing both the vertical and horizontal lengths to decrease toward an isotropic value.

(3) *Correlation of Intensity.* Analysis of the smoothed Kane Basin data shows that the intensity correlation coefficient for horizontal displacement varies with the angle φ from the propagation axis by

$$\rho \sim e^{-f^{1/2}\varphi}.$$

The intensity correlation coefficient between frequencies of ratio F (for $F>1$) varies as $\rho \sim F^{-1/4}$.

VII. REFERENCES

1. G.R. Garrison, R.E. Francois, E.W. Early, and T. Wen, "Measurements of short range sound propagation in arctic waters, 1978-1980," APL-UW 3-83, Applied Physics Laboratory, University of Washington, March 1983, Appendix A.

2. G.R. Garrison, R.E. Francois, E.W. Early, and T. Wen, "Sound absorption measurements at 10-650 kHz in arctic waters," J. Acoust. Soc. Am., **73**, 492-501 (1983).

3. R.E. Francois and G.R. Garrison, "Sound absorption based on ocean measurements: Part I: Pure water and magnesium sulfate contributions," J. Acoust. Soc. Am., **72**, 896-907 (1982). "Part II: Boric acid contribution and equation for total absorption," J. Acoust. Soc. Am., **72**, 1879-1890 (1982).

4. E.J. Skudrzyk, "Thermal microstructure in the sea and its contribution to sound level fluctuations," in *Underwater Acoustics*, V.M. Albers, Ed. (Plenum Press, New York, 1963), Lecture 12, pp. 199-233.

5. V.I. Tatarskii, *The Effects of the Turbulent Atmosphere on Wave Propagation* (English translation available from U.S. Department of Commerce, NTIS No. TT-68-50646, 1971).

6. S.M. Flatté (Ed.), R. Dashen, W.H. Munk, K.M. Watson, and F. Zachariasen, *Sound Transmission Through a Fluctuating Ocean* (Cambridge Univ. Press, Cambridge, 1979), 293 pp.

7. B.J. Uscinski, C. Macaskill, and T.E. Ewart, "Intensity fluctuations. Part I: Theory," J. Acoust. Soc. Am., **74**, 1474-1483 (1983).

8. T.E. Ewart, C. Macaskill, and B.J. Uscinski, "Intensity fluctuations. Part II: Comparison with Cobb Experiment," J. Acoust. Soc. Am., **74**, 1484-1499 (1983).

9. W.C. Meecham, M.T. Tavis, and H.T. Yura, "Born series sums for wave propagation in anisotropic random media," J. Acoust. Soc. Am., **70**, 520-534 (1981).

10. Y. Desaubies, "Note on fine structure models in underwater acoustics," J. Acoust. Soc. Am., **72**, 892-895 (1982).

11. M. Schulkin, G.R. Garrison, and T. Wen, "Acoustic variability due to layered finestructure in the Arctic," J. Acoust. Soc. Am., **66**, 235-249 (1979).

12. An excellent review of this field with a large set of recent references is given in "Small scale physics of the ocean," by D.R.. Caldwell, Reviews of Geophysics and Space Physics, **21**, 1192-1205 (1983).

13. M. Schulkin, "Intensity variance of spherical waves in anisotropic media," J. Acoust. Soc. Am., **73**, 1187-1191 (1983).

14. V.M. Komissarov, "Amplitude and phase fluctuations and their correlation in the propagation of waves in a medium with random, statistically anisotropic inhomogeneities," Sov. Phys.-Acoust., **10**, 143-152 (1964).

15. G.C. Knollman, "Wave propagation in a medium with random, spheroidal inhomogeneities," J. Acoust. Soc. Am., **36**, 681-688 (1964).

16. R.V. Ozmidov, "On the turbulent exchange in a stably stratified ocean," Atmosphere and Oceanic Physics, **1**, 493-497 (1965).

17. H. Medwin, "Sound phase and amplitude fluctuations due to temperature microstructure in the upper ocean," J. Acoust. Soc. Am., **56**, 1105-1110 (1974).

18. D.C. Whitmarsh, E. Skudrzyk, and R.J. Urick, "Forward scattering of sound in the sea and its correlation with the temperature microstructure," J. Acoust. Soc. Am., **29**, 1124-1143 (1957).

19. R.S. Andrews, "Forward scattering of underwater sound and its frequency dependence on the medium," J. Acoust. Soc. Am., **65**, 672-674 (1979).

20. J. Morison, "Internal waves in the Arctic Ocean: A Review," *Geophysics of Sea Ice* (Plenum Press, New York, in press).

21. R.F. Shvachko, "Sound fluctuations in the upper layer of the ocean and their relation to the random inhomogeneities of the medium," Sov. Phys.-Acoust., **9**, 280-282 (1964).

22. R.F. Shvachko, "Scund fluctuations and random inhomogeneities in the ocean," Sov. Phys.-Acoust., **13**, 93-97 (1967).

APPENDIX

Table A1. Coefficient of variation — Kane Basin.

No. of Runs	No. of Records	Range (m)	Frequency (kHz) 10	20	30	60	75
		(a) Harmonic method (medians)					
2	8	270	0.15	0.10	0.13	0.18	0.24
2	6	551	0.18	0.18	0.21	0.27	0.31
2	9	820	0.19	0.22	0.30	0.40	0.43
2	7	1077	0.21	0.21	0.26	0.39	0.44
		(b) Five-meter interval method (medians)					
2	9	270	0.16	0.11	0.12	0.16	0.24
2	7	551	0.16	0.14	0.15	0.20	0.26
2	10	820	0.16	0.13	0.19	0.24	0.32
2	10	1077	0.17	0.16	0.19	0.35	0.40

Table A2. Coefficient of variation determined by 5-m interval method – Chukchi Sea, 1974 (medians).

Run	Range (m)	Frequency (kHz) 10	20	30	40	60
		15 April				
18	482	0.29	0.27	0.29	0.34	0.53
19	482	0.31	0.31	0.27	0.34	0.38
20	482	0.42	0.40	0.35	0.35	0.48
21	482	0.34	0.25	0.32	0.45	0.58
30	764	0.62	0.67	0.74	0.79	0.83
31	764	0.51	0.38	0.67	0.71	0.86
32	764	0.40	0.49	0.63	0.70	0.56
23	1041	0.69	0.81	0.82	0.83	0.81
24	1041	0.82	0.86	0.80	0.80	0.77
25	1041	0.69	0.76	0.67	0.80	0.84
26	1317	0.66	0.74	0.74	0.80	0.83
27	1317	0.93	0.79	0.86	0.81	0.81
29	1317	0.55	0.65	0.79	0.80	0.71
		18 April				
38	193	0.20	0.12	0.12	0.067	0.11
39	193	0.16	0.10	0.10	0.12	0.14
40	193	0.13	0.13	0.11	0.083	0.11
42	364	0.21	0.21	0.21	0.21	0.24
47	550	0.45	0.41	0.54	0.69	0.65
48	550	0.40	0.43	0.67	0.72	0.92
50	550	0.60	0.56	0.80	0.81	0.71
51	550	0.52	0.68	0.61	0.77	0.87
52	733	0.59	0.61	0.75	0.85	0.79
55	733	0.40	0.37	0.40	0.55	0.71
56	733	0.47	0.54	0.38	0.54	0.60

Table A3. Coefficient of variation determined by harmonic method — Chukchi Sea.

Run No.	Range (m)	Depth Interval (m)	Low Spatial Wavenumber Region Acoustic Frequency (kHz) 10	20	30	40	60	High Spatial Wavenumber Region Acoustic Frequency (kHz) 10	20	30	40	60
					15 April							
18	482	14-30	0.17	0.13	0.27	0.25	0.40	0.32	0.45	0.60	0.82	0.99
19	482	14-30	0.08	0.01	0.13	0.21	0.21	0.27	0.34	0.51	0.43	0.70
20	482	10-39	0.26	0.25	0.28	0.34	0.31	0.31	0.35	0.38	0.46	0.57
21	482	18-50	0.09	0.38	0.40	0.40	0.31	0.36	0.57	0.58	0.62	0.77
30	764	10-70	0.26	0.14	0.18	0.30	0.30	0.97	1.08	1.05	1.10	0.93
31	764	10-70	0.63	0.54	0.62	0.68	0.73	0.60	0.68	0.86	1.08	1.51
32	764	15-40	0.19	0.32	0.45	0.42	0.35	0.43	0.39	0.62	0.84	0.97
23	1041	20-30	0.40	0.82	0.45	0.67	0.55	0.45	0.39	0.68	0.79	0.88
24	1041	10-70	0.55	0.38	0.46	0.38	0.51	0.72	0.97	0.88	0.92	0.88
25	1041	10-44	0.42	0.40	0.27	0.35	0.43	0.60	0.65	0.60	0.88	0.84
26	1317	20-70	0.80	0.97	0.90	0.84	0.63	0.92	0.90	1.01	1.10	0.88
27	1317	20-70	0.60	0.75	0.54	0.58	0.62	0.82	0.86	1.12	1.12	0.97
29	1317	10-35	0.58	0.70	0.53	0.58	0.49	1.01	0.97	1.08	1.14	1.20
					18 April							
38	193	24-65	0.20	0.13	0.11	0.08	0.06	0.23	0.16	0.13	0.12	0.11
39	193	24-70	0.19	0.26	0.037	0.08	0.17	0.21	0.16	0.10	0.14	0.19
42	364	18-53	0.13	0.13	0.030	0.04	0.04	0.26	0.26	0.20	0.23	0.23
47	550	17-34	0.15	0.22	0.079	0.07	0.09	0.30	0.17	0.26	0.36	0.52
48	550	11-40	0.32	0.40	0.32	0.30	0.39	0.31	0.35	0.60	0.63	0.86
50	550	14-32	0.07	0.22	0.32	0.25	0.28	0.31	0.42	0.72	0.75	0.73
51	550	18-35	0.28	0.31	0.27	0.26	0.26	0.34	0.57	0.73	0.80	0.82
52	733	10-42	0.32	0.42	0.27	0.35	0.36	0.54	0.63	0.75	0.88	0.82
55	733	10-47	0.16	0.27	0.23	0.30	0.31	0.36	0.52	0.55	0.73	0.92
56	733	10-47	0.31	0.36	0.46	0.40	0.30	0.35	0.34	0.28	0.48	0.72

Table A4. Coefficient of variation — Chukchi Sea, 1974 (medians are for data in Tables 7 and 8).

Date	No. of Runs	Range (m)	Frequency (kHz) 10	20	30	40	60
(a) Harmonic method (medians)							
15 April	4	482	0.32	0.40	0.55	0.54	0.74
	3	764	0.60	0.68	0.86	1.08	0.97
	3	1041	0.60	0.65	0.68	0.88	0.88
	3	1317	0.92	0.90	1.08	1.12	0.97
18 April	3	193	0.22	0.16	0.12	0.13	0.15
	1	364	0.26	0.26	0.20	0.23	0.23
	4	550	0.31	0.39	0.66	0.69	0.78
	3	733	0.36	0.52	0.55	0.73	0.82
(b) Five-meter interval method (medians)							
15 April	4	482	0.33	0.29	0.31	0.35	0.51
	3	764	0.51	0.49	0.67	0.71	0.83
	3	1041	0.69	0.81	0.80	0.80	0.81
	3	1317	0.66	0.74	0.79	0.80	0.81
18 April	3	193	0.16	0.12	0.11	0.083	0.11
	1	364	0.21	0.21	0.21	0.21	0.24
	4	550	0.49	0.50	0.64	0.75	0.79
	3	733	0.47	0.54	0.40	0.55	0.71

Table A5. Coefficient of variation determined by 5-m interval method — Chukchi Sea (individual runs).

Run No.	Range (m)	|θ| < 1.5° Frequency (kHz) 10	20	30	40	60	|θ| ≥ 1.5° Frequency (kHz) 10	20	30	40	60
					15 April 1974						
18	482	0.29	0.35	0.30	0.49	0.71	0.30	0.16	0.23	0.27	0.45
19	482	0.34	0.33	0.32	0.35	0.49	0.31	0.23	0.27	0.31	0.31
20	482	0.61	0.49	0.58	0.64	0.78	0.29	0.26	0.27	0.31	0.33
21	482	0.48	0.42	0.53	0.38	0.77	0.23	0.24	0.28	0.52	0.51
30	764	0.62	0.73	0.79	0.79	0.82	0.66	0.34	0.62	0.64	0.83
31	764	0.58	0.66	0.84	0.94	0.98	0.28	0.25	0.34	0.45	0.66
32	764	0.50	0.66	0.83	0.92	0.68	0.34	0.29	0.37	0.50	0.52
23	1041	0.79	0.94	0.94	0.89	0.87	0.56	0.63	0.64	0.74	0.68
24	1041	0.82	0.87	1.02	0.87	0.90	0.57	0.74	0.62	0.78	0.62
25	1041	0.73	0.82	1.11	1.11	0.94	0.54	0.53	0.48	0.79	0.81
26	1317	0.82	0.77	0.78	0.80	0.83	0.56	0.69	0.70	0.78	0.87
27	1317	0.93	0.81	0.94	0.83	0.99	0.80	0.55	0.66	0.80	0.63
29	1317	0.91	0.81	0.81	0.89	0.84	0.49	0.61	0.65	0.80	0.60
					18 April 1974						
38	193	0.19	0.13	0.095	0.033	0.085	0.20	0.12	0.12	0.080	0.13
39	193	0.15	0.11	0.086	0.13	0.13	0.20	0.10	0.11	0.12	0.16
40	193	0.13	0.13	0.11	0.077	0.094	0.13	0.13	0.13	0.092	0.14
42	364	0.17	0.17	0.19	0.19	0.22	0.26	0.25	0.22	0.26	0.26
47	550	0.57	0.54	0.83	0.82	0.73	0.26	0.23	0.39	0.47	0.59
48	550	0.48	0.85	0.91	0.81	0.99	0.29	0.27	0.39	0.48	0.57
50	550	0.71	0.75	0.92	0.88	0.77	0.22	0.33	0.60	0.77	0.68
51	550	0.80	0.81	0.78	0.90	0.91	0.31	0.56	0.58	0.64	0.85
52	733	0.60	0.63	0.76	0.86	0.62	0.51	0.58	0.74	0.66	0.82
55	733	0.41	0.37	0.42	0.58	0.73	0.34	0.37	0.30	0.35	0.39
56	733	0.65	0.66	0.68	0.70	0.84	0.42	0.44	0.31	0.52	0.49

Table A6. Coefficient of variation determined by 5-m interval method – Chukchi Sea, 1974 (medians are for data in Table A5).

Range (m)	$\|\theta\| < 1.5°$ Frequency (kHz)					$\|\theta\| \geq 1.5°$ Frequency (kHz)				
	10	20	30	40	60	10	20	30	40	60
				15 April						
482	0.41	0.42	0.43	0.44	0.74	0.30	0.24	0.27	0.31	0.39
764	0.58	0.66	0.83	0.92	0.82	0.34	0.29	0.37	0.50	0.66
1041	0.79	0.87	1.02	0.89	0.90	0.56	0.63	0.62	0.78	0.68
1317	0.91	0.81	0.81	0.83	0.84	0.56	0.61	0.66	0.80	0.63
				18 April						
193	0.15	0.13	0.095	0.077	0.094	0.20	0.12	0.12	0.092	0.14
364[a]	0.17	0.17	0.19	0.19	0.22	0.26	0.25	0.22	0.26	0.26
550	0.64	0.78	0.87	0.85	0.84	0.28	0.30	0.49	0.56	0.64
733	0.60	0.63	0.68	0.70	0.73	0.42	0.44	0.31	0.52	0.49

[a]One run only

Table A7. Coefficient of variation (median) vs elevation angle — Chukchi Sea.

Range (m)	|θ| Limits for Each 5-m Interval[a] (deg)	Frequency (kHz) 10	20	30	40	60
		15 April 1974				
482	0-0.6	0.46	0.30	0.49	0.68	0.55
	0.6-1.2	0.69	0.68	0.93	0.66	0.63
	1.2-1.8	0.39	0.32	0.25	0.29	0.55
	1.8-2.4	0.44	0.34	0.32	0.48	0.86
	2.4-3.0	0.28	0.36	0.45	0.35	0.48
	3.0-3.6	0.24	0.33	0.31	0.42	0.58
	3.6-4.2	0.31	0.23	0.28	0.33	0.37
	4.2-4.7	0.26	0.18	0.32	0.31	0.33
	4.7-5.3	0.21	0.23	0.27	0.29	0.48
	5.3-5.9	0.20	0.23	0.27	0.31	0.39
	5.9-6.5	0.26	0.19	0.21	0.29	0.42
	6.5-7.1	0.31	0.17	0.14	0.34	0.48
764	0-0.2	0.51	0.56	0.92	1.12	0.80
	0.2-0.5	0.65	0.73	0.80	0.73	0.91
	0.5-0.9	0.52	0.68	0.73	0.96	0.90
	0.9-1.3	0.43	0.51	0.84	0.87	0.77
	1.3-1.7	0.79	0.59	0.69	0.91	0.89
	1.7-2.0	0.56	0.34	0.67	0.48	0.80
	2.0-2.4	0.32	0.40	0.56	0.65	0.59
	2.4-2.8	0.32	0.33	0.49	0.83	0.53
	2.8-3.1	0.27	0.29	0.38	0.50	0.53
	3.1-3.4	0.31	0.55	0.33	0.64	0.81
	3.4-3.7	0.72	0.20	0.24	0.45	0.32
	3.7-4.1	0.21	0.20	0.29	0.38	0.49
	4.1-4.5	0.29	0.18	0.58	0.32	0.31

[a]Interval includes the lower limit but not the upper one.

Table A7, cont. Coefficient of variation (median) vs elevation angle — Chukchi Sea.

Range (m)	|θ| Limits for Each 5-m Interval (deg)	Frequency (kHz) 10	20	30	40	60
	15 April 1974					
1041	0-0.3	0.69	1.10	1.11	1.01	0.94
	0.3-0.6	0.74	0.88	0.98	0.74	0.80
	0.6-0.8	0.79	1.01	0.97	0.92	1.05
	0.8-1.1	0.97	0.84	0.98	0.97	0.89
	1.1-1.4	0.73	0.74	0.82	0.84	0.75
	1.4-1.7	0.76	0.88	0.82	0.81	1.12
	1.7-1.9	0.56	0.71	0.69	0.88	0.92
	1.9-2.2	0.52	1.10	0.73	0.75	0.84
	2.2-2.5	0.71	0.94	0.56	0.87	0.63
	2.5-2.8	0.45	0.72	0.56	0.80	0.67
	2.8-3.0	0.45	0.42	0.34	0.56	0.66
	3.0-3.3	0.38	0.30	0.51	0.72	0.61
	3.3-3.6	0.61	0.53	0.50	0.80	0.95
1317	0-0.1	0.93	0.79	0.79	0.93	0.93
	0.1-0.3	0.74	0.77	0.95	0.98	0.83
	0.3-0.5	1.10	0.83	1.10	0.80	0.82
	0.5-0.7	0.79	1.11	0.86	0.83	0.79
	0.7-1.0	0.63	0.80	0.79	0.95	0.67
	1.0-1.2	0.60	0.51	0.70	0.72	0.82
	1.2-1.4	0.56	0.62	0.68	0.78	0.51
	1.4-1.6	0.79	0.44	0.45	0.68	0.78
	1.6-2.0	0.53	0.51	0.95	0.85	0.71
	2.0-2.2	0.50	0.65	0.61	1.12	0.46
	2.2-2.4	0.39	0.77	0.29	0.44	0.58
	2.4-2.6	0.33	0.48	0.48	0.66	0.64
	2.6-2.8	0.49	0.61	0.65	0.88	0.60

Table A7, cont. Coefficient of variation (median) vs elevation angle — Chukchi Sea.

Range (m)	|θ| Limits for Each 5-m Interval (deg)	Frequency (kHz) 10	20	30	40	60
	18 April 1974					
193	0-1.5	0.22	0.13	0.11	0.08	0.11
	1.5-3.0	0.21	0.12	0.07	0.10	0.08
	3.0-4.4	0.14	0.15	0.09	0.26	0.09
	4.4-5.9	0.14	0.11	0.09	0.05	0.09
	5.9-7.4	0.17	0.12	0.10	0.08	0.12
	7.4-8.8	0.15	0.17	0.11	0.08	0.12
	8.8-10.3	0.19	0.12	0.12	0.07	0.11
	10.3-11.7	0.11	0.10	0.12	0.09	0.11
	11.7-13.1	0.13	0.09	0.13	0.07	0.16
	13.1-14.5	0.12	0.10	0.12	0.09	0.14
	14.5-15.9	0.20	0.11	0.13	0.09	0.16
	15.9-17.3	0.31	0.13	0.13	0.13	0.19
364	0-0.8	0.23	0.22	0.33	0.31	0.33
	0.8-1.6	0.28	0.19	0.25	0.24	0.38
	1.6-2.4	0.19	0.17	0.16	0.19	0.22
	2.4-3.1	0.18	0.09	0.09	0.11	0.22
	3.1-3.9	0.15	0.23	0.12	0.17	0.13
	3.9-4.7	0.24	0.25	0.24	0.31	0.29
	4.7-5.5	0.15	0.26	0.21	0.26	0.28
	5.5-6.3	0.26	0.31	0.26	0.27	0.26
	6.3-7.1	0.42	0.13	0.13	0.11	0.13
	7.1-7.8	0.44	0.21	0.22	0.22	0.19

Table A7, cont. Coefficient of variation (median) vs elevation angle – Chukchi Sea.

Range (m)	|θ| Limits for Each 5-m Interval (deg)	Frequency (kHz) 10	20	30	40	60
	18 April 1974					
550	0-0.5	0.68	0.63	0.81	0.75	0.81
	0.5-1.0	0.80	0.82	0.87	1.11	0.93
	1.0-1.5	0.70	0.81	0.68	0.78	0.90
	1.5-2.0	0.73	0.74	0.85	0.77	0.92
	2.0-2.5	0.47	0.44	0.80	0.82	0.76
	2.5-3.0	0.38	0.43	0.58	0.79	0.70
	3.0-3.5	0.30	0.28	0.33	0.60	0.74
	3.5-4.1	0.26	0.33	0.35	0.56	0.57
	4.1-4.6	0.26	0.38	0.44	0.49	0.69
	4.6-5.1	0.22	0.25	0.46	0.38	0.49
733	0-0.4	0.85	0.62	0.80	0.85	0.52
	0.4-0.8	0.67	0.17	0.26	0.42	0.47
	0.8-1.2	0.81	0.58	0.74	1.10	0.94
	1.2-1.6	0.46	0.63	0.89	0.74	0.75
	1.6-2.0	0.51	0.63	0.64	0.55	0.83
	2.0-2.3	0.63	0.65	0.42	0.59	0.76
	2.3-2.7	0.36	0.28	0.39	0.51	0.82
	2.7-3.1	0.43	0.43	0.42	0.53	0.79
	3.1-3.5	0.40	0.41	0.40	0.52	0.56
	3.5-3.9	0.31	0.54	0.60	0.80	0.93
	3.9-4.2	0.34	0.59	0.46	0.66	0.84
	4.2-4.6	0.32	0.27	0.39	0.41	0.36
	4.6-5.0	0.30	0.40	0.36	0.46	0.70
	5.0-5.4	0.31	0.28	0.24	0.38	0.54
	5.4-5.8	0.30	0.34	0.13	0.12	0.33

Table A8. Vertical correlation lengths (m) — Chukchi Sea (computed on residuals from 4-m smoothed intensity-depth profiles).

Run	Range (m)	Frequency (kHz) 10	20	30	40	60
		15 April				
18	482	3.16	2.96	2.26	1.94	1.54
19	482	5.82	2.66	1.88	1.64	1.28
20	482	4.08	3.52	2.38	1.88	1.34
21	482	3.84	2.50	3.14	2.30	1.82
31	764	4.44	2.00	1.84	1.02	1.14
32	764	3.68	2.64	2.42	1.90	1.12
23	1041	3.42	1.74	1.54	1.78	1.28
24	1041	3.48	2.54	2.30	1.80	1.46
25	1041	3.76	1.18	1.78	1.50	0.96
27	1317	2.76	1.92	1.66	1.82	1.36
29	1317	2.82	2.78	1.74	1.70	1.10
30	1317	3.54	2.26	1.96	1.52	1.12
median (m)		3.62	2.52	1.92	1.80	1.28
		18 April				
38	193	1.64	1.82	1.52	1.18	1.14
40	193	3.94	4.02	2.04	2.02	1.82
42	364	3.42	3.22	1.92	1.70	1.54
48	550	4.64	2.68	2.24	1.92	1.48
50	550	3.16	1.76	1.30	1.28	0.88
52	733	3.48	2.90	1.74	1.38	1.04
55	733	4.30	2.32	2.06	1.88	1.36
56	733	3.60	3.12	2.26	2.02	1.80
median (m)		3.54	2.80	1.98	1.80	1.42
Average of the two data sets (m)		3.58	2.66	1.96	1.80	1.36

Table A9. Refractive index variance, $\overline{\mu^2}$, for various depth intervals.

Date and Local Time	Depth Range (m)	Depth Interval (m)	$\overline{\mu^2} \times 10^9$	a_o (m)[a]
	(a) 60-m Intervals			
Chukchi Sea				
4/15/74:0820	9.68 - 70.10	60.24	269.1	7.07
4/15/74:2220	10.18 - 70.15	59.97	244.1	4.23
4/18/74:1330	10.30 - 70.02	59.72	147.4	5.92
Kane Basin				
4/10/79:0540-#97	9.63 - 70.26	60.63	7.81	6.74
4/10/79:1445-#99	9.86 - 70.49	60.63	3.85	8.55
	(b) 30-m Intervals			
Chukchi Sea				
4/15/74:0820	9.68 - 40.23	30.43	116	4.59
	40.54 - 70.10	29.56	5.84	1.52
4/15/74:2220	10.18 - 39.88	29.70	214	3.67
	40.20 - 70.15	29.95	46.3	3.10
4/18/74:1330	10.30 - 40.29	29.99	105	4.54
	40.54 - 70.02	29.48	7.10	1.31
Kane Basin				
4/10/79:0540	9.63 - 39.95	30.32	0.153	0.50
	40.41 - 70.26	29.85	5.55	3.08
4/10/79:1445	9.86 - 39.95	30.09	0.282	3.12
	40.52 - 70.49	29.97	1.04	1.90

[a] a_o, the "correlation length," is defined as the lag size on the normalized autocorrelation curve that corresponds to e^{-1} in amplitude. This differs from the definition of correlation length for intensity given in Section III.b.

Table A9, cont. Refractive index variance, $\overline{\mu^2}$, for various depth intervals.

Date and Local Time	Depth Range (m)	Depth Interval (m)	$\overline{\mu^2} \times 10^9$	a_o (m)
		(c) 20-m Intervals		
Chukchi Sea				
4/15/74:0820	9.68 - 29.93	20.07	23.6	1.91
	29.63 - 50.19	20.26	5.52	1.65
	50.44 - 70.10	19.66	5.93	1.74
4/15/74:2220	10.18 - 29.63	19.45	87.1	2.47
	29.63 - 49.77	20.14	8.79	1.41
	50.02 - 70.15	20.13	63.8	3.01
4/18/74:1330	10.30 - 29.78	19.48	33.1	2.49
	29.78 - 49.85	20.07	17.2	1.30
	49.85 - 70.02	20.17	6.04	1.17
Kane Basin				
4/10/79:0540	9.63 - 30.43	20.80	0.162	0.86
	30.43 - 49.88	19.45	2.60	2.40
	49.88 - 70.26	20.38	1.65	1.62
4/10/79:1445	9.86 - 29.97	20.11	0.238	2.39
	29.97 - 49.77	19.80	0.162	1.06
	49.77 - 70.49	20.72	0.894	1.42
		(d) 10-m Intervals		
Chukchi Sea				
4/15/74:0820	10.15 - 20.26	10.11	16.6	0.94
	20.53 - 30.20	9.67	1.51	1.13
	30.53 - 40.29	9.76	2.36	1.19
	40.54 - 50.19	9.65	3.96	0.90
	50.44 - 60.18	9.74	2.72	0.61
	60.48 - 70.10	9.62	4.61	1.01
		Medians:	3.34	0.974
4/15/74:2220	10.18 - 20.07	9.89	37.0	1.15
	20.41 - 30.20	9.79	3.97	0.82
	30.43 - 40.20	9.77	14.7	1.29
	40.46 - 50.02	9.56	1.34	0.58
	50.27 - 60.07	9.80	15.8	0.97
	60.23 - 70.15	9.92	8.66	0.94
		Medians:	11.68	0.956
4/18/74:1330	9.96 - 20.16	10.20	11.8	0.97
	20.47 - 30.02	9.55	1.59	0.99
	30.02 - 40.00	9.98	-	-
	40.29 - 50.02	9.73	5.44	0.85
	50.38 - 60.21	9.83	1.15	1.27
	60.45 - 70.02	9.57	6.97	0.99
		Medians:	5.44	0.987

Table A9, cont. Refractive index variance, $\overline{\mu^2}$, for various depth intervals.

Date and Local Time	Depth Range (m)	Depth Interval (m)	$\overline{\mu^2} \times 10^9$	a_o (m)
	(d) 10-m Intervals, cont.			
Kane Basin				
4/10/79:0540-#97	10.09 - 19.83	9.74	0.0590	0.240
	20.66 - 29.97	9.31	0.190	0.440
	30.43 - 39.95	9.52	0.0928	0.254
	40.41 - 49.88	9.47	1.06	1.22
	50.34 - 59.76	9.42	2.45	1.34
	60.33 - 70.26	9.93	0.117	0.489
		Medians:	0.154	0.465
4/10/79:1445-#99	10.33 - 19.83	9.50	0.210	1.23
	20.98 - 29.97	8.99	0.0718	1.24
	30.43 - 39.39	9.52	0.0562	-
	40.52 - 50.22	9.70	0.165	1.12
	50.68 - 59.65	8.97	0.401	0.927
	60.10 - 70.49	10.39	0.699	1.12
		Medians:	0.188	1.12
	(e) 5-m Intervals			
Chukchi Sea				
4/15/74:0820	10.15 - 15.10	4.95	2.93	0.731
	15.38 - 20.26	4.88	7.95	0.607
	20.53 - 25.13	4.60	0.78	0.676
	25.46 - 30.20	4.74	0.42	0.635
	30.53 - 35.02	4.49	0.77	0.483
	35.35 - 40.29	5.04	0.43	0.519
	40.54 - 45.25	4.71	1.10	0.442
	45.47 - 50.19	4.72	3.95	0.569
	50.44 - 55.03	4.59	1.79	0.469
	55.28 - 60.18	4.90	1.19	0.450
	60.48 - 65.03	4.55	2.15	0.483
	65.27 - 70.10	4.83	0.24	0.497
		Medians:	1.15	0.508
4/15/74:2220	10.18 - 15.10	4.92	24.0	0.655
	15.47 - 20.07	4.60	0.78	0.410
	20.41 - 25.01	4.60	0.44	0.601
	25.31 - 30.02	4.89	1.71	0.792
	30.43 - 35.25	4.82	6.99	0.696
	35.48 - 40.20	4.72	2.20	0.377
	40.46 - 45.25	4.79	1.67	0.404
	45.53 - 50.02	4.49	0.12	0.191
	50.27 - 55.00	4.73	2.33	0.396
	55.30 - 60.07	4.77	2.77	0.369
	60.23 - 65.27	5.04	3.20	0.519
	65.51 - 70.15	4.64	6.43	0.505
		Medians:	2.27	0.458

Table A9, cont. Refractive index variance, $\overline{\mu^2}$, for various depth intervals.

Date and Local Time	Depth Range (m)	Depth Interval (m)	$\overline{\mu^2} \times 10^9$	a_o (m)
	(e) 5-m Intervals, cont.			
Chukchi Sea				
4/18/74:1330	9.96 - 15.10	5.14	1.26	0.550
	15.25 - 20.16	4.91	7.90	0.733
	20.47 - 25.19	4.72	0.44	0.296
	25.46 - 30.02	4.56	0.30	0.338
	30.34 - 35.22	4.88	4.87	0.465
	35.54 - 40.29	4.75	5.11	0.268
	40.54 - 45.05	4.51	5.16	0.268
	45.33 - 50.02	4.69	5.46	0.677
	50.38 - 55.17	4.79	0.73	0.691
	55.50 - 60.21	4.71	0.052	0.183
	60.45 - 65.14	4.69	0.50	0.635
	65.48 - 70.02	4.54	3.72	0.705
		Medians:	2.49	0.508
Kane Basin				
4/10/79:0540-#97	10.09 - 14.85	4.76	0.0915	0.266
	15.31 - 19.83	4.52	0.0226	0.168
	20.06 - 24.68	4.62	0.175	0.353
	25.02 - 29.97	4.95	0.0604	0.221
	30.43 - 34.80	4.37	0.0880	0.180
	35.37 - 39.95	4.58	0.0374	0.440
	40.41 - 44.75	4.34	0.238	0.286
	45.21 - 49.88	4.67	0.0651	0.423
	50.34 - 55.00	4.66	0.0806	0.216
	55.34 - 59.76	4.42	0.418	0.580
	60.33 - 64.40	4.07	0.0690	0.376
	65.07 - 70.26	5.19	0.0972	0.349
		Medians:	0.0843	0.318
4/10/79:1445-#99	10.33 - 14.74	4.41	0.0747	0.376
	15.08 - 19.83	4.75	0.106	0.249
	20.98 - 24.45	3.47	0.0304	0.306
	25.02 - 29.97	4.95	0.0258	0.197
	30.43 - 34.68	4.25	0.0552	0.254
	35.14 - 39.95	4.81	0.0319	0.232
	40.52 - 44.87	4.35	0.0371	0.212
	45.09 - 50.22	5.13	0.119	0.641
	50.68 - 54.77	4.09	0.244	0.502
	55.45 - 59.65	4.20	0.157	0.413
	60.10 - 64.74	4.64	0.0826	0.213
	65.30 - 70.49	5.19	0.103	0.391
		Medians:	0.787	0.280

Table A10. Correlation between intensity profiles for horizontally spaced hydrophones. The profiles from 20 to 70 m were first smoothed by taking a 4-m running average.

Range (m)	Cast	Hydrophone Separation (m)	Angle (rad)	Correlation Coefficient Frequency (kHz) 10	20	30	60	75
270	Down	30	0.111	0.97	0.48	0.83	0.87	0.59
		60	0.222	0.77	0.34	0.052	0.64	0.20
		90	0.333	0.84	0.28	0.071	0.77	0.76
270	Up	30	---	----	0.24	----	----	----
		60	---	0.60	0.36	0.51	0.64	0.35
		90	---	----	0.35	----	----	----
551	Down	30	0.054	0.95	0.89	0.74	----	----
		60	0.109	0.82	0.67	0.61	0.47	0.54
		90	0.163	0.84	0.66	0.60	----	----
551	Up	30	----	0.86	0.81	0.61	----	----
		60	----	0.66	0.48	0.49	0.68	0.52
		90	----	0.66	0.29	0.45	----	----
820	Down	30	0.037	0.95	0.77	0.60	0.53	0.58
		60	0.073	0.69	0.55	0.49	0.50	0.46
		90	0.110	0.55	0.51	0.51	0.42	0.51
820	Up	30		0.81	0.83	0.81	0.69	0.75
		60		0.76	0.88	0.67	0.62	0.54
		90		0.84	0.74	0.74	0.56	0.48
1077	Down	30	0.028	0.96	0.94	0.90	0.37	-0.11
		60	0.056	0.85	0.88	0.85	0.71	0.49
		90	0.084	0.76	0.75	0.77	0.55	0.19
1077	Up	30		0.98	0.94	0.94	0.83	0.84
		60		0.87	0.79	0.70	0.67	0.69
		90		0.88	0.69	0.61	0.57	0.58

Table A11. Correlation between intensity profiles for vertically spaced hydrophones. The profiles, which were taken from 20 to 70 m, were smoothed by taking a 4-m running average.

Range (m)	Cast	Hydrophone Separation (m)	Correlation Coefficient Frequency (kHz) 10	20	30	60	75
270	Down	10	0.78	-0.01	0.28	0.40	0.09
		20	0.57	-0.49	-0.56	0.11	0.11
		30	0.34	-0.09	-0.58	-0.00	0.44
270	Up	10	0.16	0.21	-0.15	0.38	0.22
		20	0.47	0.03	0.26	0.60	0.28
		30	-0.13	-0.01	-0.13	0.63	0.21
551	Down	10	-0.19	-0.42	-0.50	-0.13	-0.13
		20	0.24	-0.09	-0.17	-0.12	0.40
		30	0.01	-0.61	-0.58	-0.31	0.20
551	Up	10	0.46	0.13	0.12	0.25	0.72
		20	0.16	-0.41	-0.02	0.01	-0.49
		30	0.28	-0.32	-0.22	-0.22	-0.32
820	Down	10	0.16	-0.33	-0.33	-0.20	-0.02
		20	-0.12	0.01	0.18	0.06	-0.02
		30	-0.47	-0.06	-0.76	-0.65	-0.66
820	Up	10	0.07	0.21	0.31	0.35	0.00
		20	-0.16	-0.0	0.14	0.28	0.40
		30	-0.09	0.23	-0.30	-0.29	-0.04
1077	Down	10	0.25	0.38	0.47	0.26	0.16
		20	-0.34	-0.12	0.034	-0.13	-0.27
		30	-0.40	-0.70	-0.66	-0.58	-0.50
1077	Up	10	0.29	0.40	0.47	0.07	0.37
		20	0.62	0.72	0.73	0.65	0.76
		30	-0.30	-0.03	0.07	-0.20	0.14

Table A12. Correlation between frequencies at each range.

Freq. (kHz)	Freq. (kHz) 10	20	30	60	75	Freq. (kHz)	Freq. (kHz) 10	20	30	60	75
R = 270 m						R = 820 m					
10	1.00	0.01	0.40	0.34	0.24	10	1.00	0.85	0.78	0.78	0.63
20		1.00	0.61	0.39	0.67	20		1.00	0.95	0.82	0.81
30			1.00	0.65	0.29	30			1.00	0.90	0.88
60				1.00	0.26	60				1.00	0.91
75					1.00	75					1.00
R = 551 m						R = 1077 m					
10	1.00	0.84	0.73	0.69	0.76	10	1.00	0.91	0.83	0.59	0.57
20		1.00	0.91	0.66	0.65	20		1.00	0.94	0.88	0.84
30			1.00	0.85	0.54	30			1.00	0.88	0.88
60				1.00	0.89	60				1.00	0.95
75					1.00	75					1.00

REPORT DOCUMENTATION PAGE

READ INSTRUCTIONS BEFORE COMPLETING FORM

1 REPORT NUMBER

2. GOVT ACCESSION NO. AD-A150550

3 RECIPIENT'S CATALOG NUMBER

4 TITLE (and Subtitle)

HIGH-FREQUENCY ACOUSTIC VARIABILITY IN THE ARCTIC

5 TYPE OF REPORT & PERIOD COVERED

Technical

6 PERFORMING ORG. REPORT NUMBER

APL-UW 8312

7 AUTHOR(s)

M. Schulkin, G.R. Garrison, T. Wen

8 CONTRACT OR GRANT NUMBER(s)

ONR: N00014-77-C-0309

NAVSEA: N00024-81-C-6042

9 PERFORMING ORGANIZATION NAME AND ADDRESS

Applied Physics Laboratory
University of Washington
1013 N.E. 40th Street, Seattle, WA 98105

10. PROGRAM ELEMENT, PROJECT, TASK AREA & WORK UNIT NUMBERS

62711N
62759N

11 CONTROLLING OFFICE NAME AND ADDRESS

Office of Naval Research, Code 425
Department of the Navy
Arlington, VA 22217

12. REPORT DATE

May 1984

13. NUMBER OF PAGES

68

14 MONITORING AGENCY NAME & ADDRESS(if different from Controlling Office)

15. SECURITY CLASS. (of this report)

Unclassified

15a. DECLASSIFICATION DOWNGRADING SCHEDULE

16 DISTRIBUTION STATEMENT (of this Report)

Distribution unlimited

17 DISTRIBUTION STATEMENT (of the abstract entered in Block 20, if different from Report)

18 SUPPLEMENTARY NOTES

This report was originally titled "Acoustic Variability Due to Arctic Finestructure."

19 KEY WORDS (Continue on reverse side if necessary and identify by block number)

High frequency acoustics, acoustic variability, acoustic intensity variance, acoustic coefficient of variation, vertical correlation length, anistropy, refractive index variance, coherence, correlation, intensity spectra, finestructure, CTD, bioacoustics, ice floe, Arctic, Kane Basin, Chukchi Sea, Arctic acoustics

20 ABSTRACT (Continue on reverse side if necessary and identify by block number)

Fluctuations in acoustic intensity have been studied for two locations in the Arctic -- the Chukchi Sea (1974) and the Kane Basin (1979) -- using the same measurement and analysis techniques. A five-frequency transducer covering the range 10-75 kHz was moved continuously in the vertical direction from 10 to 70 m. The results were used to determine the vertical correlation length and the coefficient of variation (rms variance) for the (cont.)

20., cont.

intensity at the five frequencies simultaneously. Conductivity and temperature vs depth were measured continuously before and after each set of acoustic runs. These profiles were used to construct sound ray diagrams and to compute the refractive index variance.

For direct-path propagation in both locations, it was found that when the acoustic intensity variance at low spatial wavenumbers is filtered out the remaining variance depends on the first power of the frequency and approximately the square of the range. This internal-wave-like behavior is supported by additional evidence.

The vertical correlation lengths observed for the direct-path intensity indicate that the scattering features have lifetimes longer than a few seconds and less than a few minutes. The study suggests that the scattering structures are related to anisotropic eddies that tend toward isotropy as they cascade to smaller size. Plots of a strength parameter vs a diffraction parameter show that after deterministic variations are removed from the measurements the remaining variations lie in the unsaturated direct-path region.

Distribution List

Addressee	No. of Copies
Assistant Secretary of the Navy (Research Engineering and Systems) Department of the Navy Washington, D.C. 20350	2
Chief of Naval Operations Department of the Navy Washington, D.C. 20350	
NOP-02	1
NOP-095	1
NOP-098	1
NOP-22	1
NOP-226	1
NOP-952D	1
Chief of Naval Material Department of the Navy Washington, D.C. 20360	
NMAT 07	1
NMAT 072	2
Project Manager Anti-Submarine Warfare Systems Project Office (PM4) Department of the Navy Washington, D.C. 20360	1
Director of Defense Research and Engineering Office of Assistant Director (Ocean Control) The Pentagon Washington, D.C. 20301	1
Chief of Naval Research Department of the Navy 800 North Quincy Street Arlington, Virginia 22217	1
Code 102C	1
Code 200	1
Code 420	1
Code 425	6
Commanding Officer ONR Eastern/Central Regional Office Bldg. 114 Section D 666 Summer Street Boston, Massachusetts 02210	1
Commanding Officer ONR Branch Office 536 S. Clark Street Chicago, Illinois 60605	1
Commanding Officer ONR Branch Office, London Box 39 FPO New York, New York 09510	1
Commanding Officer ONR Western Regional Office 1030 E. Green Street Pasadena, California 91106	1

Addressee	No. of Copies
Commander Naval Air Systems Command Headquarters Department of the Navy Washington, D.C. 20361	2
Commander Naval Electronic Systems Command Hq. Department of the Navy Washington, D.C. 20360	1
NESC 03	1
PME 124	1
Commander Naval Sea Systems Command Department of the Navy Washington, D.C. 20362	1
Code 06	1
Code 06B	3
Code 63R	1
Code 63R1	2
Code 63R3	1
Code 63R34	2
Code 632	1
Code 99612	14
Code PMS-402	1
Commander Naval Weapons Center China Lake, California 93555	
Library	1
Commander Naval Ocean Systems Center San Diego, California 92152	
Library	4
Code 19	2
Code 5311	1
Code 6351	1
Code 65	1
Code 712	1
Code 7124	1
Commander Naval Air Development Center Warminster, Pennsylvania 18974	1
Commander David W. Taylor Naval Ship Research and Development Center Bethesda, Maryland 20084	1
Code 1905.2	1
Commander Naval Surface Weapons Center White Oak Silver Spring, Maryland 20910	
Mr. M.M. Kleinerman	1
Library	2
Code R-43	1
Code U06	2

Addressee	No. of Copies
Commander, SECOND Fleet Fleet Post Office New York, New York 09501	1
Commander, THIRD Fleet Fleet Post Office San Francisco, California 96601	1
Commander Submarine Force U.S. Atlantic Fleet Norfolk, Virginia 23511	2
Commander Submarine Force U.S. Pacific Fleet N-21	1
FPO San Francisco, California 96601	1
Commander Submarine Squadron THREE Fleet Station Post Office San Diego, California 92132	1
Commander Submarine Group FIVE Fleet Station Post Office San Diego, California 92132	1
Commander Submarine Development Squadron TWELVE Box 70 Naval Submarine Base - New London Groton, Connecticut 06340	1
Director Defense Advanced Research Project Agency 1400 Wilson Boulevard Arlington, Virginia 22209	1
Commanding Officer Naval Intelligence Support Center 4301 Suitland Road Washington, D.C. 20390	1
Director of Navy Laboratories Crystal Plaza, Bldg. 5 Washington, D.C. 20360	1
Commanding Officer Naval Coastal Systems Center Panama City, Florida 32407	1
Commanding Officer Naval Underwater Systems Center Newport, Rhode Island 02840	1
Library	5
Code 3341	1
Code 363	2
Commanding Officer Naval Ocean Research and Development Activity NSTL Station, Mississippi 39529	1
Code 100/110	1
Code 113	2
Code 115	1
Code 125L	1
Code 240	1
Code 300	1
Code 323	1
Code 332	1
Code 343	1
Code 345	1
Code 500	1

Addressee	No. of Copies
Commanding Officer Naval Oceanographic Office NSTL Station, Mississippi 39577	1
Commander Naval Oceanography Command NSTL Station, Mississippi 39522	1
Director, Liaison Office Naval Ocean Research & Development Activity 800 North Quincy Street Arlington, Virginia 22217	1
Commanding Officer Naval Submarine School Box 700 Naval Submarine Base - New London Groton, Connecticut 06340	1
Superintendent Naval Postgraduate School Monterey, California 93940	
Library	2
Dr. H. Medwin	1
Commanding Officer Naval Environmental Prediction Research Facility Monterey, California 93940	1
Office of the Director Naval Oceanography Division (OP-952D) Navy Department Washington, D.C. 20350	2
Commanding Officer Fleet Numerical Ocean Center Monterey, California 93940	1
Commander Naval Facilities Engineering Command Headquarters 200 Stovall Street Alexandria, Virginia 22332	1
Officer-in-Charge New London Laboratory Naval Underwater Systems Center New London, Connecticut 06320	2
Library	1
Code 3302	2
Dr. Ding Lee	1
Director Naval Research Laboratory Washington, D.C. 20375	
Technical Information Division	3
Code 5109	1
Code 8168	1
Dr. C. Votaw	1
Director Applied Research Laboratory Pennsylvania State University State College, Pennsylvania 16801	1
R. Ingram	2
Dr. S. McDaniel	1

Addressee	No. of Copies
Director Applied Research Laboratories The University of Texas at Austin P.O. Box 8029 10000 FM Road 1325 Austin, Texas 78712	2
Director Applied Physics Laboratory University of Washington 1013 Northeast 40th Street Seattle, Washington 98105	
Mr. R.E. Francois	1
Dr. G.R. Garrison	1
Dr. M. Schulkin	4
Mr. C.G. Sienkiewicz	1
Mr. T. Wen	1
Library	1
Director Woods Hole Oceanographic Institution Woods Hole, Massachusetts 02543	1
Dr. Y.J.F. Desaubies	1
Director Scripps Institution of Oceanography P.O. Box 6049 San Diego, California 92106	1
Dr. C.S. Cox	1
Polar Research Laboratory, Inc. 123 Santa Barbara Street Santa Barbara, California 93101	1
Office of Naval Technology 800 North Quincy Street Arlington, Virginia 22217	
Capt. John Harlett	1
University of Wisconsin Dept. of Geology & Geophysics Weeks Hall for Geological Sciences Madison, Wisconsin 53706	
Prof. C.S. Clay	1
Science Applications, Inc. 205 Montecito Avenue Monterey, California 93940	
Dr. W.W. Denner	1
Dr. C.W. Spofford	1
Massachusetts Institute of Technology Department of Ocean Engineering Cambridge, Massachusetts 02139	
Dr. I. Dyer	1
University of California Physics Department Santa Cruz, California 95064	
Dr. S.M. Flatté	1
Georgia Institute of Technology Atlanta, Georgia 30332	
Dr. P.H. Rogers	1

Addressee	No. of Copies
Tracor, Inc. 9150 Chesapeake Drive San Diego, California 92123	
Dr. V. Holliday	1
Rensselaer Polytechnic Institute Troy, New York 12180	
Dr. M.J. Jacobson	1
Dr. W.L. Siegmann	1
University of Cambridge Department of Applied Mathematics and Theoretical Physics Silver Street Cambridge CB39EW England	
Dr. B. Uscinski	1
Columbia University Lamont-Doherty Geological Observatory Palisades, New York 10964	
Dr. H.W. Kutschale	1
The Catholic University of America Department of Civil Engineering Washington, D.C. 20064	
Dr. J. McCoy	1
University of California, Los Angeles School of Engineering & Applied Science Los Angeles, California 90024	
Dr. W.C. Meecham	1
Office of Naval Research, Resident Representative University District Bldg., Room 315 1107 N.E. 45th Street Seattle, Washington 98105	1

END

FILMED

3-85

DTIC